공학박사학위논문

복합재료 액상 성형 공정에서 입자 필터링 현상에 대한 평가 및 모델링

Assessment and Modeling of Particle Filtration during the Liquid Composite Molding Process

2014년 2월

서울대학교 대학원

기계항공공학부

염 상 혁

복합재료 액상 성형 공정에서 입자 필터링 현상에 대한 평가 및 모델링

Assessment and Modeling of Particle Filtration during the Liquid Composite Molding Process

지도교수 이 우 일

이 논문을 공학박사 학위논문으로 제출함

2013 년 10 월

서울대학교 대학원

기계항공공학부

염 상 혁

염상혁의 공학박사 학위논문을 인준함

2013 년 12 월

위 원 장 : 조 맹 효

부위원장 : 이 우 일

위 원 : 안 성 훈

위 원 : 유 웅 렬

위 원 : 김 승 모

Assessment and Modeling of Particle Filtration during the Liquid Composite Molding Process

Sang Hyuk Yum
School of Mechanical and Aerospace Engineering
Seoul National University

Abstract

Numerous filler particles are being developed and applied to improve the properties of conventional composite materials or to develop composite materials with additional functionalities. When filler particles are added to the polymer matrix of a fiber-reinforced composite material, the particles dispersed in the polymer resin can be filtered between fiber strands during the manufacturing process, which leads to a nonuniform particle distribution and material defects. Therefore, understanding and controlling such filtration phenomena has become a critical issue. In the present study, a new microscopic methodology for measuring the distribution of filler particles in

fully cured composite parts using an electron probe microanalyzer (EPMA) is proposed. The distributions of spherical titanium dioxide particles and carbon nanotubes conjugated with silver nanoparticles as tracers were visualized by elemental mapping analysis. Furthermore, the concentrations were separately measured in the intratow and intertow regions by quantitative analysis. Effects of the critical parameters of the manufacturing process on filtration were investigated. Numerical analysis was also performed to observe the spatial distribution of the filler particles and effects of process parameters over larger range which experimental analysis could not cover. A model for filtration rate was suggested in the form of the function of crucial variables such as permeability of porous media, resin viscosity, pressure gradient and concentration of particles according to the results of the analysis.

Keywords: Particle filtration, Nanocomposites, Electron probe micro analyzer (EPMA), Resin transfer molding (RTM)

Student Number: 2008-30193

Table of contents

List of Figures

List of Tables

1. Introduction

1.1. General description about advanced composite materials

Composite materials consist of two or more distinct phases, where one serves as binder and the other as reinforcement. They have been used for constructive purposes and synthetic composites became popular during the second half of the 20th century. Wood consists of cellulose fibers and lignin matrix, and is the representative natural composites which has been used throughout the human history. The first use of manmade composites is straw-reinforced clay bricks that was used for construction of buildings in the ancient Egypt. Also in South and Central America the pottery was made with the reinforcements of plant fibers. These early uses of fibrous reinforcements were maybe used to keep the clay from cracking during drying process, rather than improving the mechanical properties as in modern applications. Nowadays, composite materials are used to produce high performance and light weight parts in various areas such as automotive and aircraft manufacturing, boat industry and sports equipment. Composite materials are usually made from epoxy, vinylester or polyester matrices reinforced by glass or carbon fibers. The advantages of such composite materials are the outstanding mechanical properties such as strength and stiffness per

weight, the possibility to have anisotropic properties and that they are easily formed into complex structures. Their light weight can result in less fuel consumptions for aircrafts and automotives.

In recent years, advanced composite materials have been developed in order to meet increased demands of light weight, high quality and cost effective materials from the manufacturers of high performance structures. They have functionalities such as thermal resistance, electromagnetic shielding, sensor properties, self-healing properties or better conductivity integrated into the conventional composite materials. Integration of functionality into composite structures not only reduces additional parts which can result in saving in structural weight but also decrease the production costs since the functional material can be made in one single process. These functional properties can be added in several ways. One is the functional layers inside the composite structure, another way is to apply the functional fibers as reinforcements. And a third way is to mix functional filler-particles into the resin prior to injection. Especially, results of increased thermal properties and fire resistance were reported by applying this technique. Introducing particle-added resin not only introduced additional functional properties but often also improved the mechanical properties of the materials. The general requirements for this kind of material is the minimum amount of defects Moreover, for composites with integrated functionality it is essential to produce materials with uniform distributions of the particles and their functionality. To meet

this requirement, an extensive control of the manufacturing process is necessary, since poor distribution can cause defects leading to poor mechanical properties or functional properties of the particle-added composite materials.

1.2. Overview and problem description

Advanced composite materials are widely used owing to their superior characteristics such as light weight, chemical resistance, and high vibration damping. The utility of these composites can be further enhanced by adding filler particles to the matrix resin.

When filler particles are added to fiber-reinforced composite materials, they may be subjected to filtration by the fibrous reinforcement. This is especially true for manufacturing processes involving extensive resin flow, such as the liquid composite molding (LCM) process. The particles in the suspension can undergo filtration through porous media. The filtered particles narrowing and clogging the flow channels may cause some disadvantages such as low permeability, long mold-filling times, and void formation in the fiber preform. In addition, the filler particles cannot be distributed uniformly through the final composite part, and this leads to a nonuniform distribution of the corresponding properties of the material, let alone increased production costs. Therefore, it is crucial to understand the mechanism of such filtration phenomena so

that a model for predicting and controlling the distribution of particles in composite materials can be developed. Such a model should be able to predict the distribution of the filler particles under various processing conditions. In order to do so, it is essential to develop a methodology for measuring the concentrations of filler particles in a fully cured composite product.

1.3. Literature review

Filler particles can improve the mechanical properties or conductivity of conventional composites, while other functional particles can be added to introduce new functionalities such as self-healing [1] or photovoltaic properties [2]. Carbon nanotubes (CNTs) in particular are popular filler particles owing to their notable mechanical properties [3] and high thermal and electrical conductivities [4, 5]. Many researchers have reported enhancements in these properties in CNT-containing composites [6, 7], and new functions such as electromagnetic shielding [8] and fire resistance [9] have been introduced. . The particles in the suspension can undergo filtration through porous media by physical capture, the action of electrostatic forces, or van der Waals forces between the particles and the filter surface [10]. In the manufacturing of polymer matrix composite materials with low Reynolds numbers, the high viscosity and low

velocity cause the drag force exerted on the particles by the resin flow to be dominant, and physical capture acts as the main mechanism. Consequently, the ratio of particle size to pore size becomes the critical factor influencing the filtration mechanism. Cake filtration occurs when the particle size is larger than the pore size. The particles are filtered in front of the fibrous pore and accumulate, forming a cake. On the other hand, very small particles flow freely inside the fibrous preform, and little filtration takes place. For an intermediate ratio of particle size to pore size, deep bed filtration is the main mechanism. The particles are deposited gradually, and the flow channels become narrow. As a result, cake filtration may start to occur.

Numerous studies on the filtration of suspensions over porous media have been performed in a variety of application areas such as water purification and waste treatment. Only a few studies, however, have dealt with the filtration of particles through fibrous reinforcements during the manufacture of composite materials. A direct numerical simulation technique was developed to describe particulate flows and the deposition of particles in which Stokes–Brinkman coupling along with the hydrodynamic interaction between particles and the fluid were employed to describe the flow in dual-scale porous media [11]. Voronoi discretization and minimization of the dissipation rate of energy were used to study fluid-flow-driven motion of particles and it was introduced to investigate the two-dimensional particle flow and filtration through arrays of fiber bundles [12, 13]. Furthermore, a semi-analytical model

describing the motion of fibrous particles was used for analysis of the displacement and orientation of dispersed carbon nanotubes during impregnation of dual-scale fabrics [14]. A simulation model based on an Eulerian multiphase flow approach was used to investigate the flow characteristics of carbon-nanoparticle-filled fluids, and the interactions between the microfiber walls and the nanoparticle additives were studied [15]. Later, a model for a nanoparticle-filled fluid based on the Lagrangian multiphase approach was introduced to predict the nanoparticle trajectories and their interactions with the fluid flow and microfiber walls [16]. A macroscopic filtration model based on the sieve mechanism, in which large particles accumulate in front of small pores was proposed to predict the concentration distribution of particles within the dual-scale fibrous media, [17]. The authors also performed an experimental study on the behavior of microparticles in the dual-scale woven preform to validate the model. The suspension was injected along the perpendicular direction of the piled fiber mats, and the amount of filtered particles within each layer was measured by rinsing the layers and straining the resulting solution to collect the particles (Figure 1). Microscopic imaging and microparticle image velocimetry (micro-PIV) measurements (Figure 2) were employed to investigate the filtration using a colorless glycerol/water mixture and fluorescent micron-sized particles [18]. Unfortunately, in the two studies mentioned above, the measurements were performed on liquid suspensions and not on fully cured, solid parts. Furthermore, the methods suffered from limitations in terms of liquid type

or size of the particles. Another macroscopic model was proposed to analyze filtration during resin transfer molding (RTM) in which the conservation of mass was coupled with Darcy's law and the particle retention kinetics [19]. This was then improved to take liquid retention into account [20]. In another paper, an enhanced model was proposed to consider the evolution of the viscosity and the permeability [21]. The authors validated the models with experimental investigations measuring the concentration of particles in fully cured parts using a so-called "burn-off" test. Samples were cut from a certain composite part, and both the matrix and fiber material of each sample was burned off so as to measure the mass of the filtered microparticles. Here, synthetic PET fibers were used as the reinforcement, as these fibers could be completely removed by calcination, while glass microbeads were used as the filler owing to their nonflammable nature (Figure 3). Still, the type of material used had clear limitations, and microscopic observation was not feasible. In a cured part made of resin-transfer-molded nanoclay/glass/epoxy disks, the spatial distribution of nanoclay clusters was characterized by image analysis of the SEM images and microscopic elemental analysis using wavelength dispersive spectrometry (WDS) performed of an electron probe microanalyzer (EPMA) [22].

For CNTs in particular, it has been exceedingly difficult to observe filtration phenomena experimentally, because CNTs are made up of carbon atoms, as are the constituents of most polymer resins. Therefore, when CNTs are added as filler particles

in the polymer matrix, elemental analysis cannot distinguish between the two components. Although some researchers have investigated CNT filtration phenomena in fibrous media using SEM and TEM [23], these methods only provide qualitative information and do not evaluate the part as a whole (Figure 4).

1.4. Research Objective and scope

The final objective of this research is to develop the technique to make uniform distribution of filler particles or that with certain gradient in the particle-added composite materials. To achieve this, it is essential to develop the method to measure the particle concentration and distribution inside the cured composite parts, and then the effects of process parameters on the filtration should be understood in order to control this phenomena (Figure 5).

In the present study, we developed a new methodology for measuring the distribution of filler particles in fully cured composite parts via elemental analysis using an EPMA. Mapping analysis was performed for the element making up the filler particles, and the resulting image, in combination with an SEM image showing the fiber geometry, gave a visual representation of the distribution of the filler. Quantitative analysis using WDS provided by the EPMA was also performed in order to measure the particle

concentration in the composite parts. This method could be applied to particle sizes ranging from nanometers to micrometers, and it was separately applied to the intratow and intertow regions successfully. In addition, CNTs conjugated with silver nanoparticles were used so that they could be traced via elemental analysis using the EPMA. Numerical analysis validated some of the experimental results and covered broader range of critical process parameters in order to observe their effects on filtration phenomena.

2. Experimental

2.1. Materials

The suspension used as the matrix resin consisted of epoxy and filler particles. The epoxy system consisted of a bisphenol-A-type resin and an amine-based hardener (KFR-130/KFH-140, Kukdo Chemical, South Korea). The viscosity of the mixture was 300 cP at room temperature. Spherical titanium dioxide particles (Alfa Aesar, USA) with an average diameter of 1 μm or CNT-silver particles were used as the filler. The CNT-silver powder consisted of multiwalled CNTs ranging from 10 to 15 nm in diameter and 10 to 20 μm in length, with silver nanoparticles with an average diameter of 30 nm conjugated to the CNT walls (Bioneer HQ, South Korea). The mass ratio of CNT to silver was 30:70. FE-SEM images and selected specifications of the filler particles are shown in Figure 6 and Table 1, respectively.

Dual-scale fiber mats consisting of E-glass and carbon fiber were used (Han Kuk Fiber, South Korea and Han Kuk Carbon, South Korea) as the fibrous preform. The flow channels inside the fibrous media can be classified into two categories: an intertow region and an intratow region. The channel width of the intertow region may be up to several hundreds of microns, while that of the intratow region is several microns. The

average diameter of a single strand of glass fiber is 17 μm, while that of the carbon fiber is 7 μm.

2.2. Dispersion process

To disperse the TiO_2 or CNT-silver filler particles in the resin, the epoxy was dissolved and diluted in acetone or in isopropyl alcohol, respectively. The filler particles were then mixed and dispersed using an ultrasonicator (with a CV 505 power supply and a CV 33 convertor, Sonics & Materials Inc., USA) for 10 hours for TiO_2 particles and for 7 hours for CNT-silver powder. The solvent was then evaporated in an ultrasonication bath (SD-D300H SeongDong, South Korea) to maintain the dispersion state. Finally, the suspension was placed in a convection oven to completely evaporate the solvent (Figure 7).

2.3. Dynamic light scattering measurement

The particle-size distribution of the CNT-Ag particles was measured by a dynamic light scattering (DLS) device (Zetasizer Nano ZS, Malvern, UK) in order to investigate

the state of dispersion of the particles in the epoxy resin prior to injection (Figure 8). As for TiO_2 particles, a reliable result could not be obtained because of their large size, over the micron scale, which caused remarkable sedimentation during the DLS measurement. The resin with dispersed CNT-silver particles was diluted by methyl ethyl ketone (MEK) and a stabilizer was added to keep the dispersed particles from agglomerating (DISPERBYKE 2150, BYKE, Germany) [22]. The DLS device used in this research is able to measure the particle size in a range from 1 nanometer to 5 micrometers. Because even a few agglomerates larger than the upper limit could interrupt reliable measurements, we eliminated them using a centrifugation process at 9600 g for 10 min.

2.4. Confirming the stability of conjugation between silver nanoparticles and CNTs

In the present study, silver nanoparticles conjugated to CNTs are used to trace the distribution or concentration of the particles in the polymer matrix. Thus, it is essential to investigate stability of the conjugation between the silver nanoparticles and the CNTs. CNT-silver particles were dispersed using ultrasonicator in isopropyl alcohol without the resin. Under such conditions, the particles suffered more damage than

those dispersed in the epoxy resin. Afterward, the particles were dried and FE-SEM observations were performed to confirm the conjugation state. In addition, the fracture surface of a cured composite part including CNT-silver particles was observed by FE-SEM.

2.5. Resin transfer molding

After dispersion, the hardener was added to the resin and evacuated for 20 min to eliminate air voids. The suspension was then injected under a constant pressure of 1 atm into a mold filled with the fiber perform (Figure 9), and the fiber volume fraction over the mold cavity was 0.3 in every experiment. The dimensions of the mold cavity were 70 × 160 × 5 mm^3 (w × l × d). After it was filled, the resin was cured at 70 °C for 6 h in a convection oven.

2.6. Electron probe microanalyzer measurements and post processes

For measurement, samples with a size of 5 × 5 × 5 mm^3 (w × l × d) were extracted from the fully cured composite part (Figure 10). Seven samples were cut in the

direction of resin injection and mounted in transparent epoxy for EPMA measurements. The samples were successively ground and polished using silicon carbide papers of 800 to 4000 grit and diamond paste (particle diameter = 1 or 3 μm) on a polishing cloth (Struers, Denmark).

The EPMA (JXA-8900R, JEOL, Japan) device also provides scanning electron microscopy (SEM) and light microscopy images so that the measurement location can be selected (Figure 11). Its mapping analysis visualizes the distribution of each element in the selected area, and the WDS enables precise quantitative analysis of the elements on a specimen. EPMA is, therefore, a convenient tool for investigating the distribution and concentration of filler particles in particle-containing composite materials. Elemental analyses were performed using the EPMA on the same cross section as in the SEM image, as shown schematically in Figure 10, in order to map the particle distribution or quantitatively measure the particle concentrations in the fully cured composite parts. The penetration depth of the electron beam into the sample surface is known to exceed 1 μm.

Mapping of the elements corresponding to the filler particles was conducted over an area of 300 × 300 μm^2, while the grid size was 1 × 1 μm^2. The Ti mapping showed the TiO_2 distribution, while the Ag mapping showed the CNT-silver distribution. The resulting image was then merged with the SEM image taken over the same area representing the fiber geometry using a graphics editing program (Adobe Photoshop

CS). The black backgrounds in the two images were removed before they were merged. In the merged image, the distribution of filler particles between individual reinforcing fibers was visualized (Figure 12).

The particle concentration was obtained by measuring the weight percentage of Ti or Ag measured by the quantitative WDS analysis. The electron beam size for this quantitative analysis was set to 100 μm. In the intertow region with its wide flow channel of hundreds of microns, the concentrations of TiO_2 and CNT-silver particles can be determined in wt% simply by:

$$C(\mathrm{TiO_2})_{\mathrm{intertow}} = \frac{M_{\mathrm{r}}(\mathrm{TiO_2})}{M_{\mathrm{r}}(\mathrm{Ti})} C(\mathrm{Ti}) \tag{1}$$

$$C(\mathrm{CNT\text{-}silver})_{\mathrm{intertow}} = \frac{1}{w_{\mathrm{silver}}} C(\mathrm{Ag}) \tag{2}$$

where the relative molecular masses of TiO_2 and Ti are $M_r(\mathrm{TiO_2}) = 79.866$ and $M_r(\mathrm{Ti}) = 47.867$, respectively, and C(Ti) and C(Ag) are the weight percentages of Ti and Ag, respectively, measured by the WDS on the composite part. The mass fraction of silver nanoparticles relative to the total mass of the CNT-silver product used in this research is $w_{\mathrm{silver}} \approx 0.7$.

On the other hand, in the intratow region with its narrow flow channel of several microns, the electron beam for measurement always included some fiber strands

(Figure 13). Therefore, to obtain the particle concentration in the polymer matrix in the intratow region, the area covered by the fibers among the measurement area should be calculated and excluded, namely:

$$C\left(\mathrm{TiO_2}\right)_{\mathrm{intratow}} = \frac{\frac{M_\mathrm{r}\left(\mathrm{TiO_2}\right)}{M_\mathrm{r}\left(\mathrm{Ti}\right)} C\left(\mathrm{Ti}\right)}{1-\frac{A_\mathrm{f}}{A_\mathrm{t}}} \tag{3}$$

$$C\left(\mathrm{CNT\text{-}silver}\right)_{\mathrm{intratow}} = \frac{\frac{1}{w_{\mathrm{silver}}} C\left(Ag\right)}{1-\frac{A_\mathrm{f}}{A_\mathrm{t}}} \tag{4}$$

where A_f/A_t is the ratio of the area covered by the fibers to the total measurement area.

In the presence of E-glass fibers, A_f/A_t was determined after each measurement by:

$$\left(\frac{A_\mathrm{f}}{A_\mathrm{t}}\right)_{\mathrm{GF}} = \frac{1}{w_{\mathrm{SiO_2}}} \frac{M_\mathrm{r}\left(\mathrm{SiO_2}\right)}{M_\mathrm{r}\left(\mathrm{Si}\right)} C\left(\mathrm{Si}\right) \tag{5}$$

where the mass fraction of SiO_2 to the total mass of the E-glass product used in this research is w_{SiO_2} = 0.552, the relative molecular masses of SiO_2 and Si are $M_r(\mathrm{SiO_2}) = 60.0843$ and $M_r(\mathrm{Si}) = 28.0855$, respectively and C(Si) is the weight percentage of the element Si measured by the WDS on the composite part.

When carbon fibers were used, the weight percent of the element C measured by the

WDS could not be used to determine the area covered by the fibers, since the fibers shared carbon with the epoxy matrix. Instead, we found A_f/A_t approximately by counting the number of carbon fiber strands N_f inside the electron beam area (D_{beam} = 100 μm) in the SEM image:

$$\left(\frac{A_f}{A_t}\right)_{CF} = \frac{\frac{\pi}{4} D_f{}^2 N_f}{\frac{\pi}{4} D_{beam}{}^2} \tag{6}$$

where the average diameter of one fiber strand was D_f = 7 μm. We determined this value as the average of 60 such calculations.

2.7. Results and Discussion

2.7.1. Particle-size distribution of filler particles dispersed in resin

In Figure 14, the particle-size distribution for the CNT-silver particles in the suspension after the dispersion process shows bimodal behavior. The left peak appears in the submicron range and corresponds to the well-dispersed particles, while the right peak corresponds to agglomerated particles. Even though the measured volume percentages

may not exactly represent the real distribution because of the changes during dilution in the solvent and the centrifugation process before the DLS measurement, it can be concluded that some particles were in a well-dispersed state while others were in an agglomerated state [22]. It may be also expected that the particle-size distribution of TiO_2 particles has similar bimodal behavior.

2.7.2. Stability of conjugation between silver nanoparticles and CNTs

Figure 15a shows that CNT-silver particles dispersed in isopropyl alcohol by the ultrasonicator for 7 hours have stable conjugation between the silver nanoparticles and CNTs, and Figure 15b also confirms that several silver nanoparticles are conjugated well with the CNTs on the fracture surface of the cured composite part. In addition, images of the distribution of silver nanoparticles obtained by EPMA mapping analysis for Ag (Figure 18a and b) reflect incomplete dispersion of the CNT-silver particles. This was also evidence of stable conjugation between nanoparticles and CNTs; otherwise, the nanoparticles detached from the CNTs might have had a uniform distribution over the domain.

2.7.3. Mapping of filler particle distribution in fully cured composite parts

Imaging of the particle distribution in the fibrous media was conducted using several combinations of materials, as listed in Table 2. In the images, circles of grey color are reinforcing fibers, while the other colors depict the concentration of the filler particles according to the legend on the right side of the figure. The white background represents regions of very low concentration under the detection limit of the WDS measurement. A red arrow in each image represents the flow direction.

The mapping analysis results for the particle distribution show that the dominant mechanism of filtration varied between cake filtration (Figure 16a), deep bed filtration (Figure 16b) and deposition mechanism (Figure 16c) of very small particles in the condition of high Reynolds number which does not occur in this research, according to the ratio of the particle size to the pore size. As described in the section above, filler particles dispersed in the epoxy resin were classified into two categories according to the state of dispersion: well-dispersed particles and clusters of particles [22]. Clusters of particles were mostly captured by fibers through cake filtration, while well-dispersed particles were deposited progressively on the fiber walls by deep bed filtration.

The distribution of TiO_2 particles with an average diameter of 1 μm and a

concentration of 10 wt% is plotted in Figure 17a. On the right side of the image, which corresponds to the intertow region with its wide flow channel, well-dispersed particles were distributed quite uniformly, as shown by the blue color. The clusters of particles are shown as spots mostly of light blue or of other colors. Accumulations of particles were observed both inside the fiber bundles and at the interface between the intertow and intratow regions [12, 13, 18]. The particle accumulation on the fiber walls mostly resulted from deep bed filtration of the well-dispersed particles, while the clusters of particles were filtered at the narrow flow channels through cake filtration. It can also be seen that inside the fiber bundle, particle-free resin or resin with few particles was present, as shown by the white region behind the fibers where many particles were filtered [18].

Figure 17b shows the results when carbon fibers were used as the reinforcing fibers. Many particles were filtered on the right side of the interface between the intertow and intratow regions during the resin flow into the fiber bundle [12, 13, 18]. Carbon fibers exhibited narrower channels for resin flow than did the glass fibers, so the particles had more difficulty in moving into the fiber bundles. As a result, the filler content in the intratow region was lower than that observed with glass fibers, and the white regions of particle-free resin or resin with few particles were found in broad areas at the boundary through which the resin flow went out of the fiber bundle [18], as well as inside the bundle.

When 1 wt% CNT-silver particles were added, only a few particles were observed in the intratow region, whereas a large number of particles were deposited near the interface in both Figure 18a and b, as similarly reported in a computational investigation [14]. This was because CNTs with high aspect ratios were easily filtered while moving into the fiber bundle. Furthermore, the CNT-silver particles were distributed irregularly even in the intertow region, likely because of the lower degree of dispersion of entangled nanotubes. As shown in Figure 18a, even when glass fibers with large flow channels were used, the particles were filtered vigorously at the interface between the intertow and intratow regions, as compared to when spherical particles were used. Consequently, only a small amount of well-dispersed particles could enter the glass fiber bundle. Figure 18b shows that the particles in the highly dispersed state were found to be suspended or filtered even in the quite narrow channels inside the carbon fiber bundle, which implies that advanced dispersion treatment will increase the infiltration of CNTs into the intratow region.

Future works will investigate the effects of parameters such as dispersion time and fiber orientation on the distribution or filtration of filler particles, and the method presented here is expected to serve as a convenient analysis tool.

2.7.4. Quantitative determination of filler particle concentration in fully cured

composite parts

The concentration of the filler particles was measured by quantitative EPMA analysis, and the results were plotted to present the spatial distribution of the particles in the produced material. Specifically, the values at seven different locations in two different fibrous regions along the resin flow were measured, where one value represents the average of more than ten measurements. The first value in each graph obtained (Figure 19 and 20) represents the concentration at the point before the suspension entered the fibrous media during the injection process. Notably, this value was smaller than the actual concentration of the particles after preparation of the suspension, presumably because of the incomplete dispersion of the filler particles in the polymer matrix. As a result, a fraction of the total particle content which existed as agglomerated particles were only sparsely dispersed throughout the material and, therefore, not detected by the EPMA measurements [22].

Figure 19a and b illustrate the concentrations over composite parts produced using TiO_2 particles. The graphs show that a nearly uniform distribution was obtained in the intertow region throughout the part in each graph, because there was little filtration of dispersed particles in the large flow channels [22]. However, the values observed for the intratow region for the glass fibers showed some variation because of the filtration

and ensuing accumulation of the particles inside the fiber bundle. The concentrations in the intratow region for carbon fibers were quite low, because the particles could not enter the fiber bundle through the narrow channels between the fiber strands.

The concentrations of the CNT-silver particles were also plotted versus location, as shown in Figure 20a and b. In the intertow region, the concentrations were generally uniform (as seen in both the graphs), as was also apparent in previous SEM and TEM observations [23]. This is because the particles moved freely without being subject to filtration through the wide flow paths between fiber tows [14]. The regions with large error bars reflect lower dispersion states compared to those in the case of spherical particles. The concentrations in the intratow region, on the other hand, had fairly random distributions and were generally lower than those observed in the intertow region. When carbon fibers were used (Figure 20b), the concentrations were much lower because the particles could not readily penetrate the intratow region, and the comparably small error bars are attributed to infiltration of highly dispersed particles into the narrow channels of the carbon fiber bundle.

2.7.5. Effects of process parameters on the filtration of particles

Using the methodology proposed above we investigated the effects of some critical

parameters in manufacturing process on the filtration of filler particles during the injection flow (Table 3 and 4). The concentration values measured in the inter-tow region were almost uniform over the whole part, while those in the intra-tow region varied according to the process condition. Bigger particles were filtered more in the intra-tow region as higher standard deviation of particle content in that region was found in Figure 21. And higher initial concentration of particles resulted in active filtration inside the tow as seen in Figure 22. Meanwhile, fiber orientation normal rather than parallel to flow direction caused more filtered particles in the intra-tow region as we can see in Figure 23. When the particle-added resin was injected more, particles accumulated in the tow region more due to filtration occurred for a longer time, as seen in Figure 24. The results mentioned until now are the case of spherical particles. In the case that CNT-silver particles were used as filler particles, dispersion process time was an important parameter affecting the filtration in the intra-tow region, as seen in Figure 25. When the carbon fiber with narrower flow channel was used as reinforcements, the particle concentration inside the fiber tow was quite low due to active filtration at the boundary region while entering the tow as seen in Figure 26.

3. Numerical analysis

3.1. Overview

The Lagrangian discrete phase model used in ANSYS FLUENT is explained here, shortly. The Lagrangian discrete phase model follows the Euler-Lagrange approach. The fluid phase is treated as a continuum by solving the Navier-Stokes equations, while the dispersed phase is solved by tracking a large number of particles, bubbles, or droplets through the calculated flow field. The dispersed phase can exchange momentum, mass, and energy with the fluid phase. This approach is made considerably simpler when particle-particle interactions can be neglected, and this requires that the dispersed second phase occupies a low volume fraction. The particle or droplet trajectories are computed individually at specified intervals during the fluid phase calculation. This makes the model appropriate for the modeling of spray dryers, coal and liquid fuel combustion, and some particle-laden flows, but inappropriate for the modeling of liquid-liquid mixtures, fluidized beds, or any application where the volume fraction of the second phase cannot be neglected. The trajectory of a discrete phase particle is predicted by integrating the force balance on the particle, which is written in a Lagrangian reference frame. This force balance equates the particle inertia

with the forces acting on the particle.

3.2. Verification of experimental results

The results of spatial distribution of filler particles obtained by experimental analysis using EPMA were verified by numerical analysis. A domain of dual-scale porous media made of fibrous preform was designed similarly to real fibrous media, and only at the boundary of each fiber tow filtration occurred in this analysis. Figure 27 shows that the effect of resin viscosity on the spatial distribution of particle concentrations. Both numerical and experimental results inform that low viscosity of resin enhanced the inertial effect and active filtration near the entrance region took place. And the higher tow permeability was, the more particles were filtered as seen in Figure 28. It is because the fiber tow of high permeability causes high velocity of resin flow into the tow which resulted in active filtration at the boundary region. And Figure 29 and 30 shows that the particle tracking solutions obtained in the flow field solved beforehand, in the two cases mentioned above, respectively. The lower resin viscosity was or the higher tow permeability was, the more particles were filtered, as it was expected.

3.3. Parametric study on the filtration of particles during the injection stage

The effects of resin viscosity, injection pressure and tow permeability on the filtration of particles were investigated by numerical scheme. First, the resin viscosity was almost independent to the rate of filtration except when the viscosity was quite low as shown in Figure 31. It is because flow field solution is very similar and the drag force of the resin flow on the particle is so dominant that particles could rarely break away from the streamline over the most range of viscosity as seen in Figure 32. Then injection pressure also was found to be independent to the filtration in most range of this parameter while the amount of filtered particles increased with pressure gradient in the range of low viscosity as shown in Figure 33. And the rate of filtration increased with tow permeability over the entire values of this parameter dealt in this analysis. Finally, the larger the particle diameter was the more particles were filtered in the middle range of resin viscosity, while the particle size had no effect on the filtration in the other ranges as seen in Figure 34. Particle tracking results in the above cases were shown in Figure 29, 30, 35, 36 and 37. The model for filtration of filler particles was suggested below according to above results.

$$\frac{\partial \sigma}{\partial t} = k(1-\sigma)^m \tag{7}$$

where σ represents the total amount of filtered particles and k is a function of permeability K, pressure gradient ΔP, viscosity μ and particle diameter d. k_0, n, l, q are the constants.

$$k = k_0 \mathrm{K}^n \tag{8}$$

$$k = k_0 \mu \mathrm{K}^n (\Delta P)^l d^q \quad (\mu <<) \tag{9}$$

The percentage of filtered particles was plotted again with respect to the Reynolds number as seen in Figure 38. We can see that inertia effect is dominant in the range of high Reynolds number while it is not effective when the number is low.

3.4. Random injection of filler particles

Numerical tool for particle tracking used in this research provides uniform distribution of initial position when the particles are injected into the fibrous media. However, the particle have random and irregular distribution at the entrance and this point can cause different result from the experimental approach. Therefore, we tried random injection of filler particles by generating random number of initial position at the starting line of

2-dimensional domain, and the result of final distribution of particles are plotted together with the experimental result in Figure 39. The result coincide with the experimental result better than the case of uniform injection. In this calculation, the resin viscosity was 30 cP, the tow permeability was 3.00E-10 m^2 and the injection pressure was 1 atm.

3.5. Verification of the numerical scheme: mesh sensitivity

In order to verify the convergence of the numerical calculation, we repeated the same calculation changing the mesh size and the velocity values obtained at the same point were plotted in Figure 40.

4. Conclusion

In this study, we proposed a methodology for studying the distribution of filler particles in fully cured, fiber-reinforced composite parts using elemental mapping and quantitative analysis based on EPMA and SEM measurements. The method was applied to the analysis of spherical TiO_2 particles. Moreover, even though CNTs and the polymer both consist of carbon, the method could be applied to the analysis of CNTs by employing silver-nanoparticle-conjugated CNT particles. The combined results of the mapping analysis and the SEM images acquired in the same domain helped us visualize the distribution of the filler particles within the fibrous medium. Furthermore, the particle concentrations could be quantitatively assessed by EPMA analysis in the direction of the resin flow. From this method, the spatial distributions inside and outside the fiber bundle, over the entire composite part, could be obtained. It was found that the distribution of the filler particles varied according to the particle size and particle shape as well as the fiber diameter. The proposed methods are expected to be useful for further research into the movement and filtration of filler particles during resin flow inside fibrous media. Furthermore, the parametric study on the critical process variables affecting the filtration of filler particles was performed by experimental analysis and numerical scheme. Finally a filtration model was suggested according to the relation between the parameters of manufacturing process and the

filtration rate.

References

[1] White SR, Sottos NR, Geubelle PH, Moore JS, Kessler MR, Sriram SR, et al. Autonomic healing of polymer composites. Nature. 2001;409(6822):794-797.

[2] Gupta S, Zhang QL, Emrick T, Russell TP. "Self-corralling" nanorods under an applied electric field. Nano Letters. 2006;6(9):2066-2069.

[3] Qian D, Wagner GJ, Liu WK, Yu M-F, Ruoff RS. Mechanics of carbon nanotubes. Applied Mechanics Reviews. 2002;55(6):495-533.

[4] Kim P, Shi L, Majumdar A, McEuen PL. Thermal transport measurements of individual multiwalled nanotubes. Phys Rev Lett. 2001;87(21).

[5] Ebbesen TW, Lezec HJ, Hiura H, Bennett JW, Ghaemi HF, Thio T. Electrical conductivity of individual carbon nanotubes. Nature. 1996;382(6586):54-56.

[6] Spitalsky Z, Tasis D, Papagelis K, Galiotis C. Carbon nanotube-polymer composites: Chemistry, processing, mechanical and electrical properties. Prog Polym Sci. 2010;35(3):357-401.

[7] Biercuk MJ, Llaguno MC, Radosavljevic M, Hyun JK, Johnson AT, Fischer JE. Carbon nanotube composites for thermal management. Appl Phys Lett. 2002;80(15):2767-2769.

[8] Li N, Huang Y, Du F, He XB, Lin X, Gao HJ, et al. Electromagnetic interference (EMI) shielding of single-walled carbon nanotube epoxy composites. Nano Letters. 2006;6(6):1141-1145.

[9] Kashiwagi T, Du FM, Douglas JF, Winey KI, Harris RH, Shields JR. Nanoparticle networks reduce the flammability of polymer nanocomposites. Nat Mater. 2005;4(12):928-933.

[10] Kim M-m, Zydney AL. Theoretical analysis of particle trajectories and sieving in a two-dimensional cross-flow filtration system. Journal of Membrane Science. 2006;281(1–2):666-675.

[11] Hwang WR, Advani SG, Walsh S. Direct simulations of particle deposition and filtration in dual-scale porous media. Composites Part a-Applied Science and Manufacturing. 2011;42(10):1344-1352.

[12] Frishfelds V, Lundstrom TS. Modelling of particle deposition during impregnation of dual scale fabrics. Plast Rubber Compos. 2011;40(2):65-69.

[13] Lundström T, Frishfelds V. Modeling filtration of particulate flow during impregnation of dual-scale fabrics. Journal of Composite Materials. 2012.

[14] Hogberg SM, Lundstrom TS. Motion of dispersed carbon nanotubes during impregnation of fabrics. Plast Rubber Compos. 2011;40(2):70-79.

[15] Elgafy A, Lafdi K. Carbon nanoparticle-filled polymer flow in the fabrication of novel fiber composites. Carbon. 2006;44(9):1682-1689.

[16] Elgafy A, Lafdi K. Engineering solution in monitoring nanoparticle-fluid flow during nanocomposites processing. J Nanopart Res. 2007;9(3):441-454.

[17] Chohra M, Advani SG, Gokce A, Yarlagadda S. Modeling of filtration through multiple layers of dual scale fibrous porous media. Polymer Composites. 2006;27(5):570-581.

[18] Nordlund M, Fernberg SP, Lundstrom TS. Particle deposition mechanisms during processing of advanced composite materials. Composites Part a-Applied Science and Manufacturing. 2007;38(10):2182-2193.

[19] Erdal M, Guceri SI, Danforth SC. Impregnation molding of particle-filled preceramic polymers: Process modeling. Journal of the American Ceramic Society. 1999;82(8):2017-2028.

[20] Lefevre D, Comas-Cardona S, Binetruy C, Krawczak P. Modelling the flow of particle-filled resin through a fibrous preform in liquid composite molding technologies. Composites Part a-Applied Science and Manufacturing. 2007;38(10):2154-2163.

[21] Lefevre D, Comas-Cardona S, Binetruy C, Krawczak P. Coupling filtration and

flow during liquid composite molding: Experimental investigation and simulation. Composites Science and Technology. 2009;69(13):2127-2134.

[22] Aktas L, Dharmavaram S, Hamidi YK, Altan MC. Filtration and breakdown of clay clusters during resin transfer molding of nanoclay/glass/epoxy composites. Journal of Composite Materials. 2008;42(21):2209-2229.

[23] Fan Z, Hsiao K-T, Advani SG. Experimental investigation of dispersion during flow of multi-walled carbon nanotube/polymer suspension in fibrous porous media. Carbon. 2004;42(4):871-876.

Figures

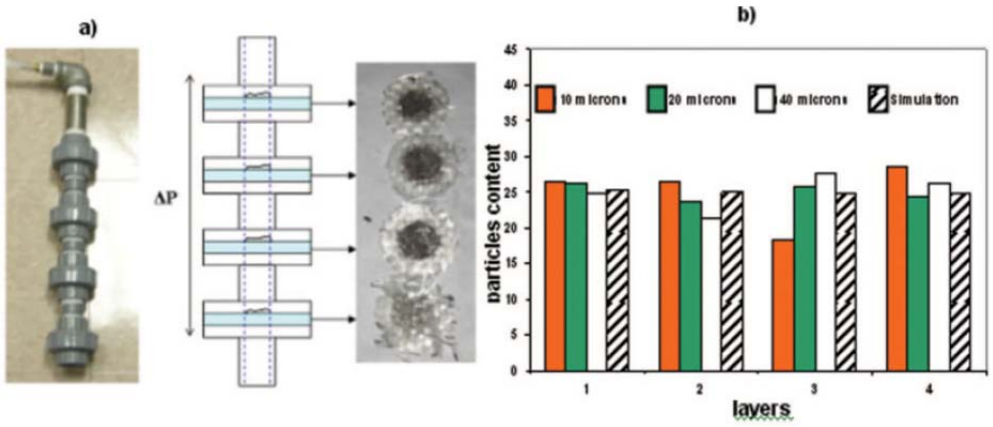

Figure 1 Example of method to measure the filtered particles by rinsing the fiber mat of each layer.

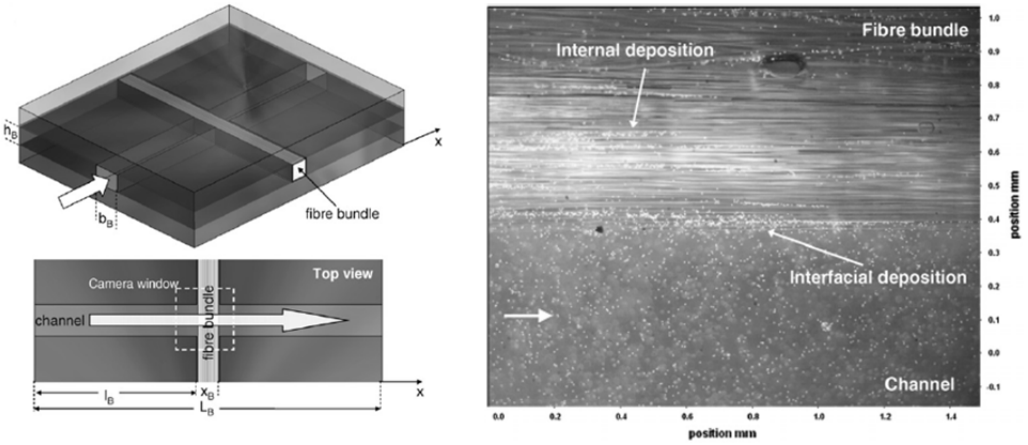

Figure 2 Example of method to measure the filtered particles by micro-PIV system and microscopic imaging.

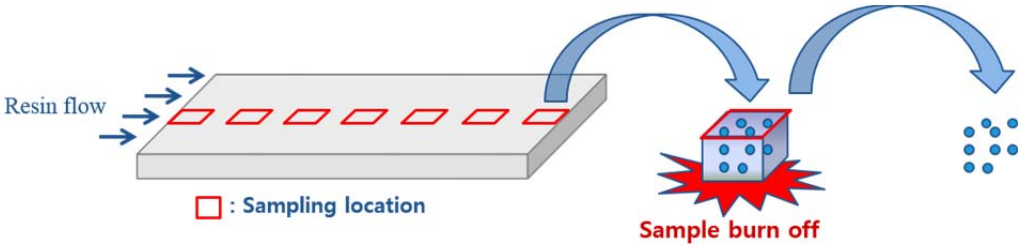

Figure 3 Example of method to measure the filtered particles by burning the cured parts and collecting the particles.

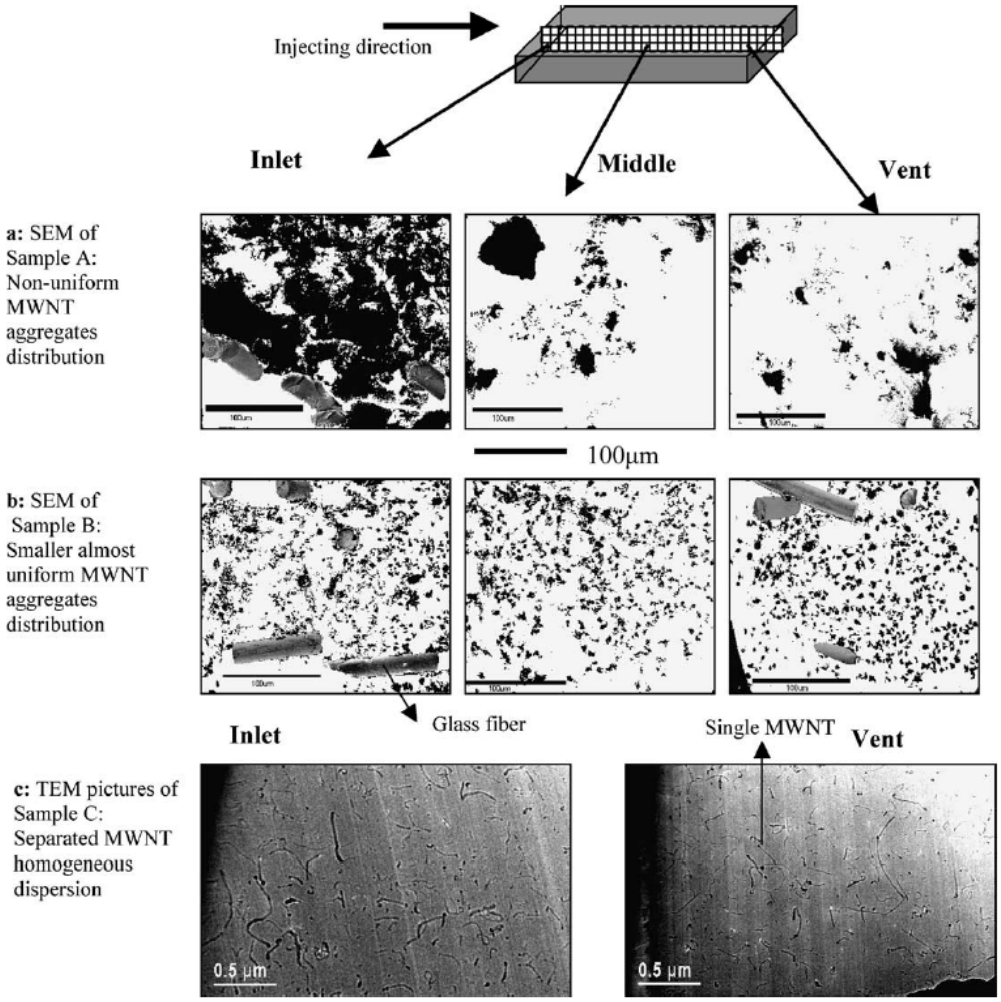

Figure 4 Example of method to measure the filtered particles by SEM and TEM measurements.

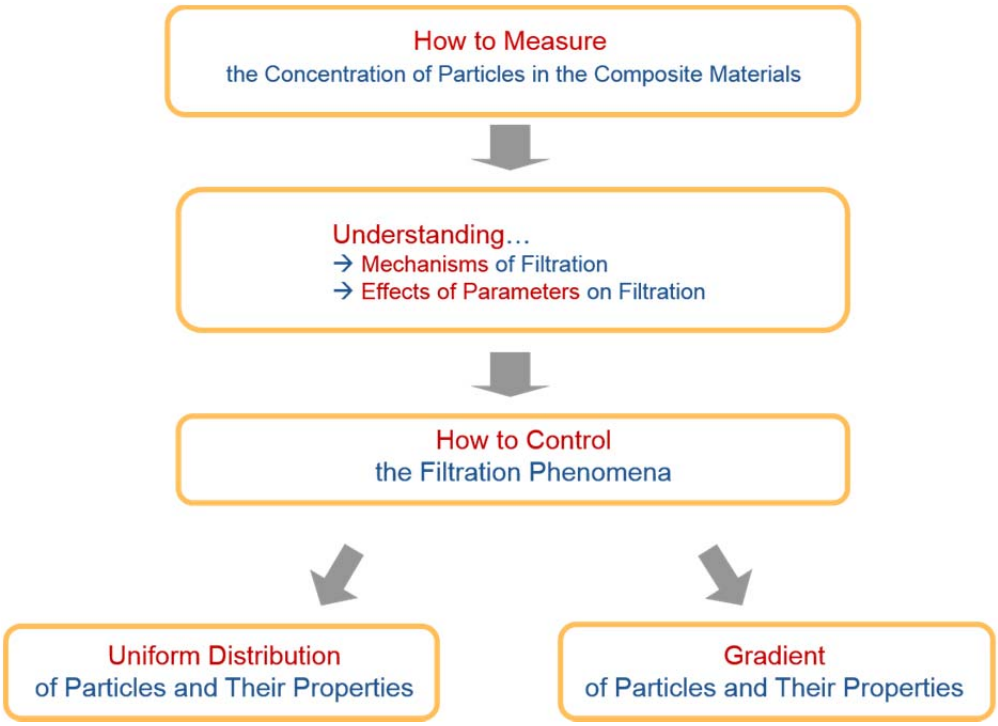

Figure 5 Objective and strategy of this research.

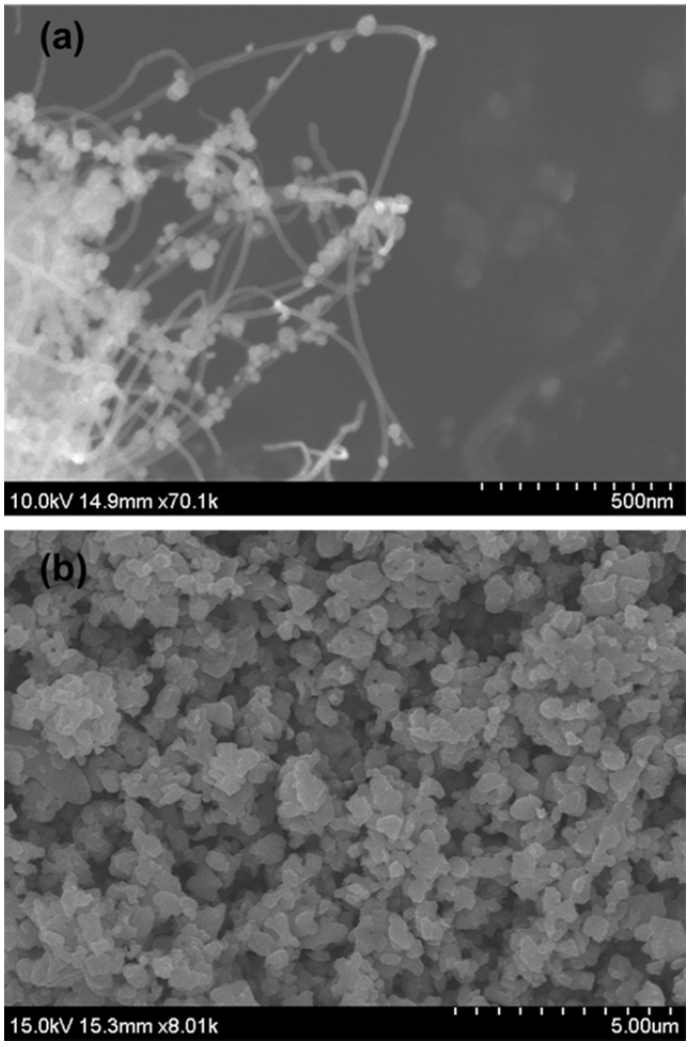

Figure 6 FE-SEM image of (a) CNT-silver particles and (b) TiO_2 particles with an average diameter of 1 μm

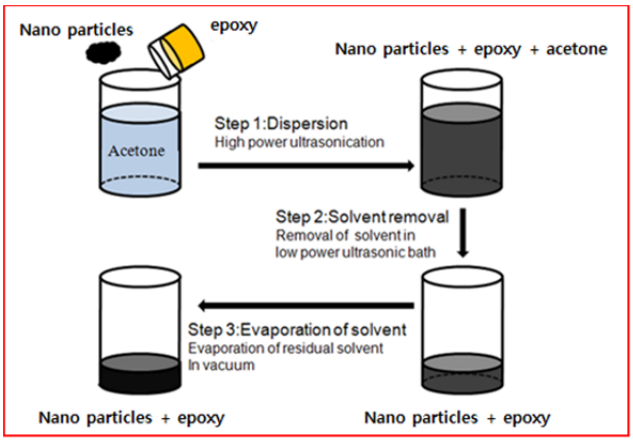

Tip-type ultrasonicator

Figure 7 Dispersion process for filler particles by dilution of resin using a solvent and ultrasonication energy.

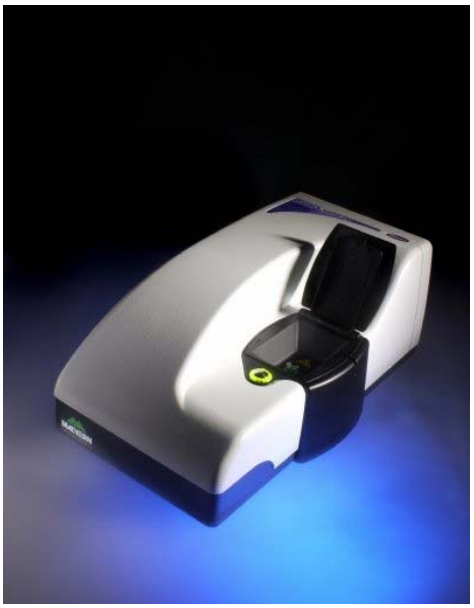

Figure 8 Dynamic light scattering (DLS) device.

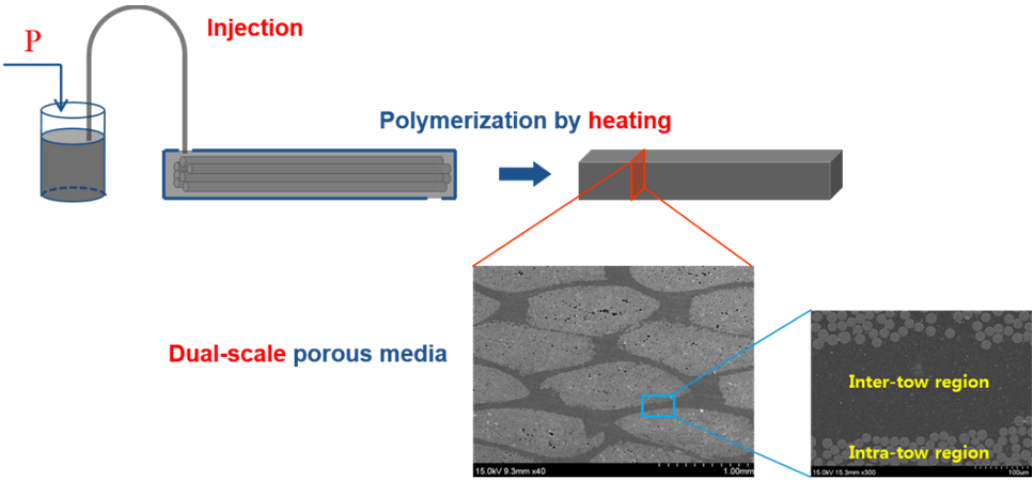

Figure 9 Injection stage by resin transfer molding process.

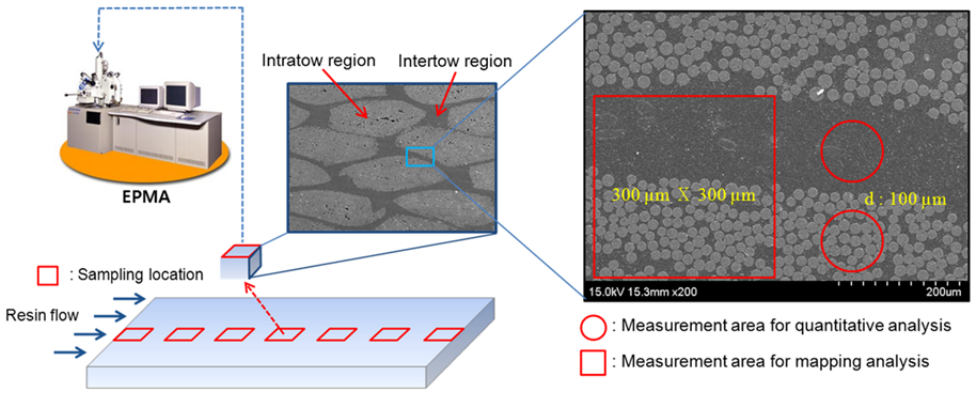

Figure 10 Schematic representation of the sampling process and EPMA measurement of the filler particle distribution in the cross-sectioned cured composite part.

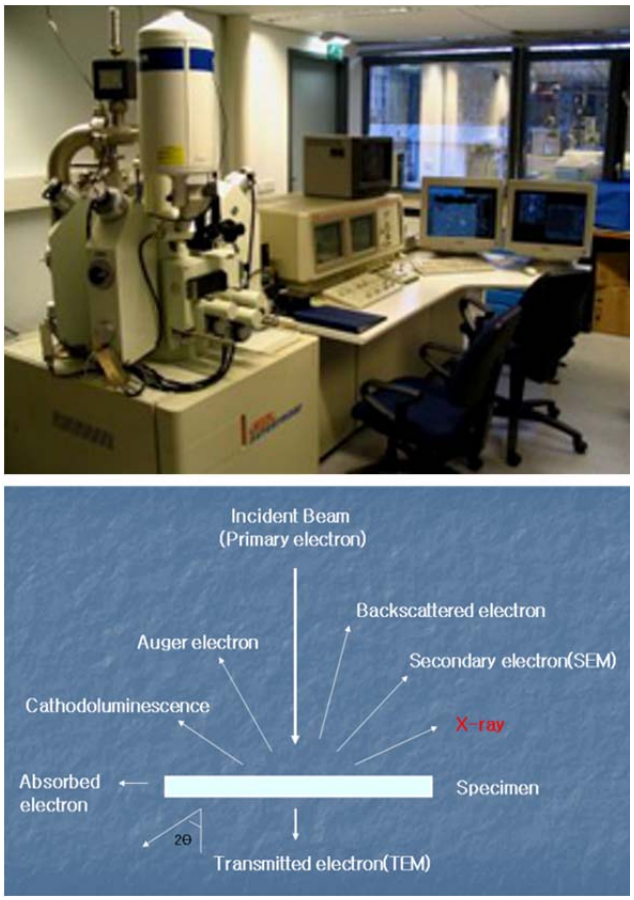

Figure 11 EPMA device and its principle to measure the concentration of each element on the specimen.

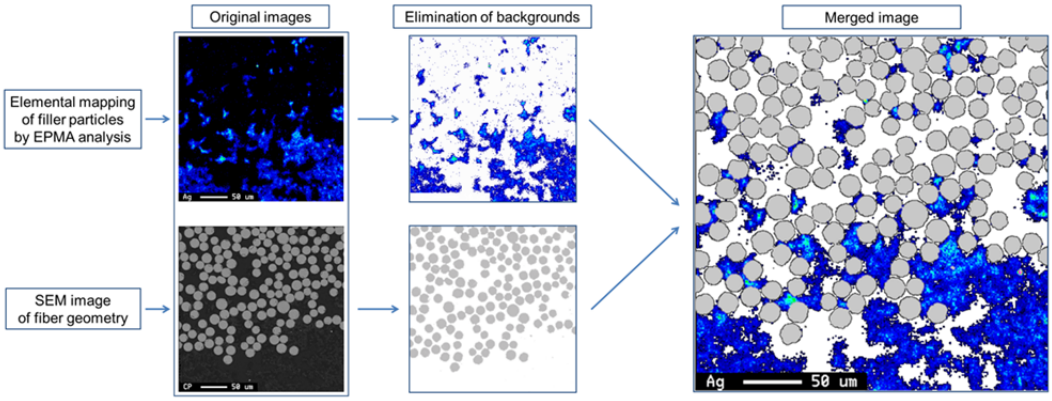

Figure 12 Example of merging the result of elemental mapping of filler particles and the SEM image of the fiber geometry in the cross-sectioned cured composite part including CNT-silver particles and glass fibers.

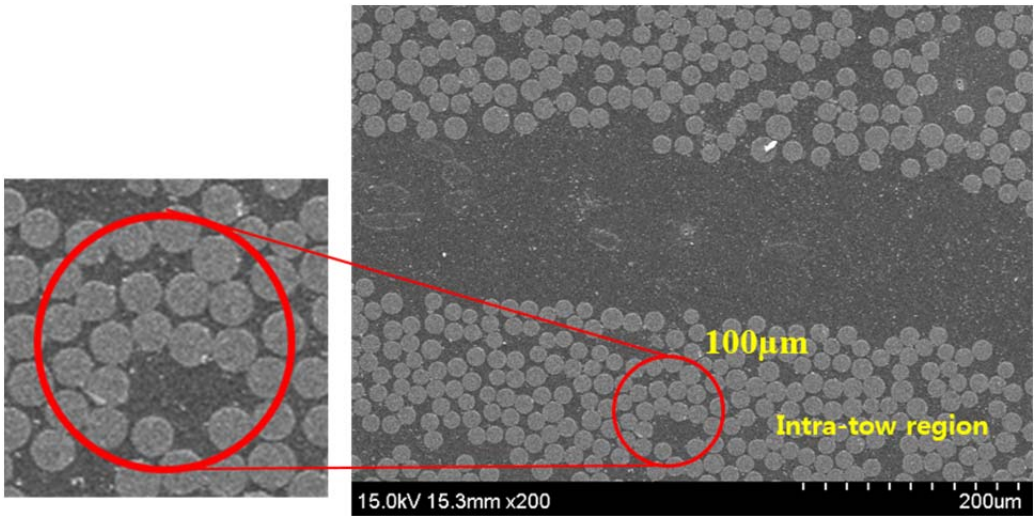

Figure 13 EPMA measurement in the intra-tow region in which the reinforcing fibers are included in the measuring area.

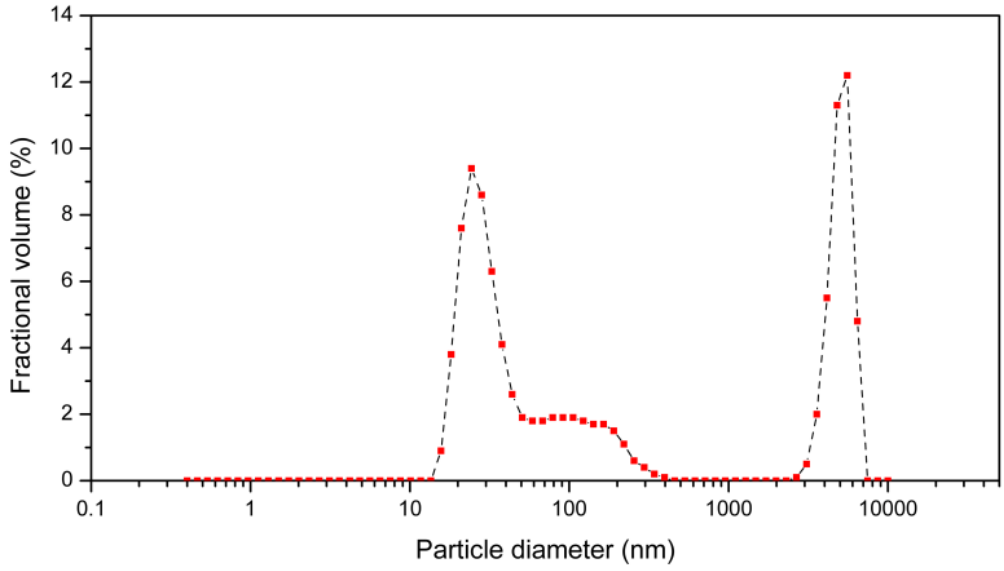

Figure 14 Dynamic light scattering result on the particle-size distribution of CNT-silver particles dispersed in epoxy resin after dilution with methyl ethyl ketone including an additive for stabilization.

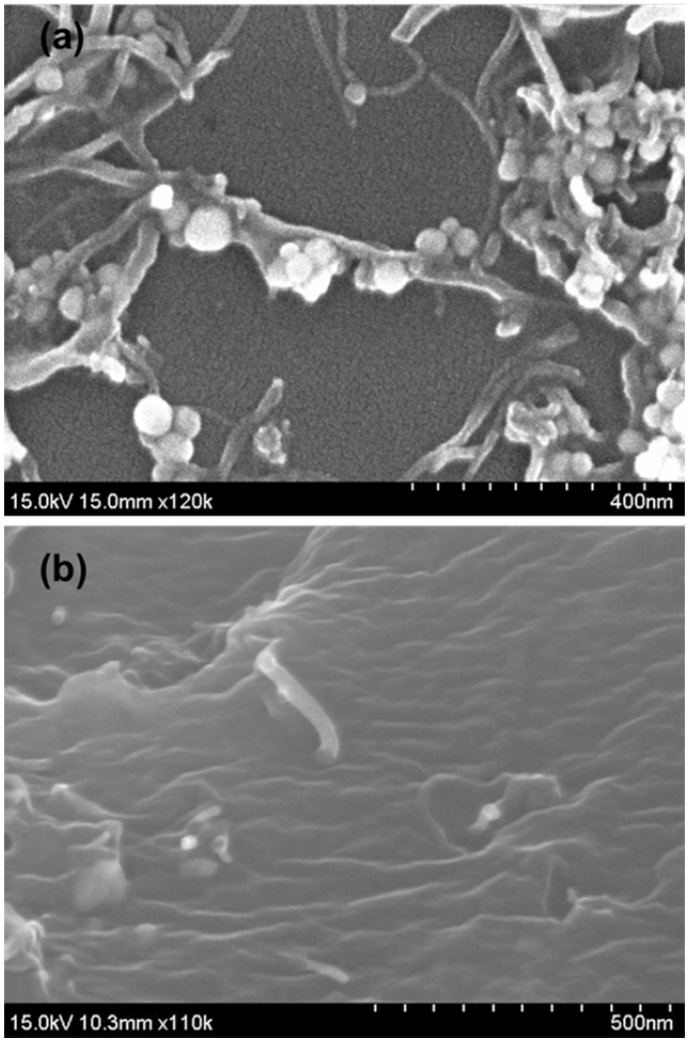

Figure 15 FE-SEM image of (a) CNT-silver particles treated by ultrasonication for 7 hours and (b) CNT-silver particles on the fracture surface of the cured composite part.

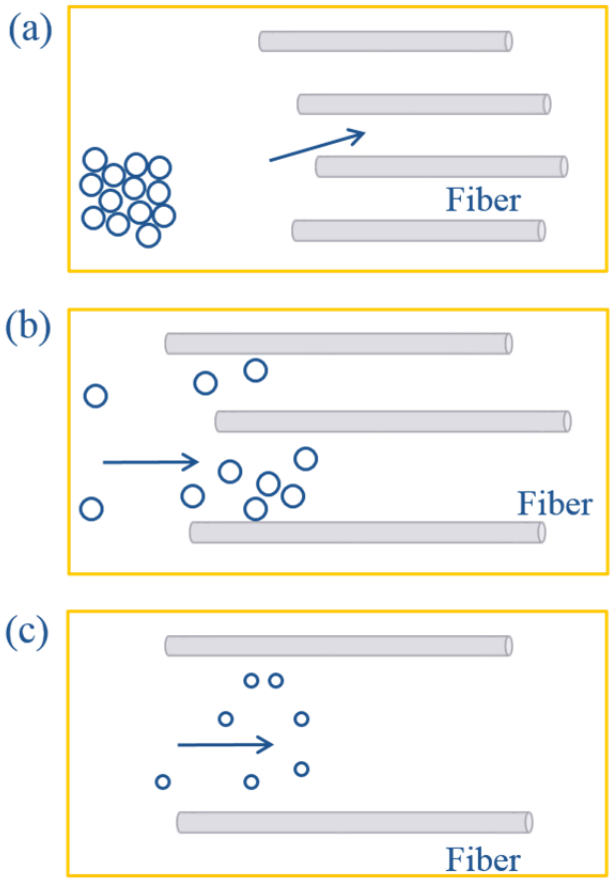

Figure 16 Three mechanisms of particle filtration inside the fibrous preform.

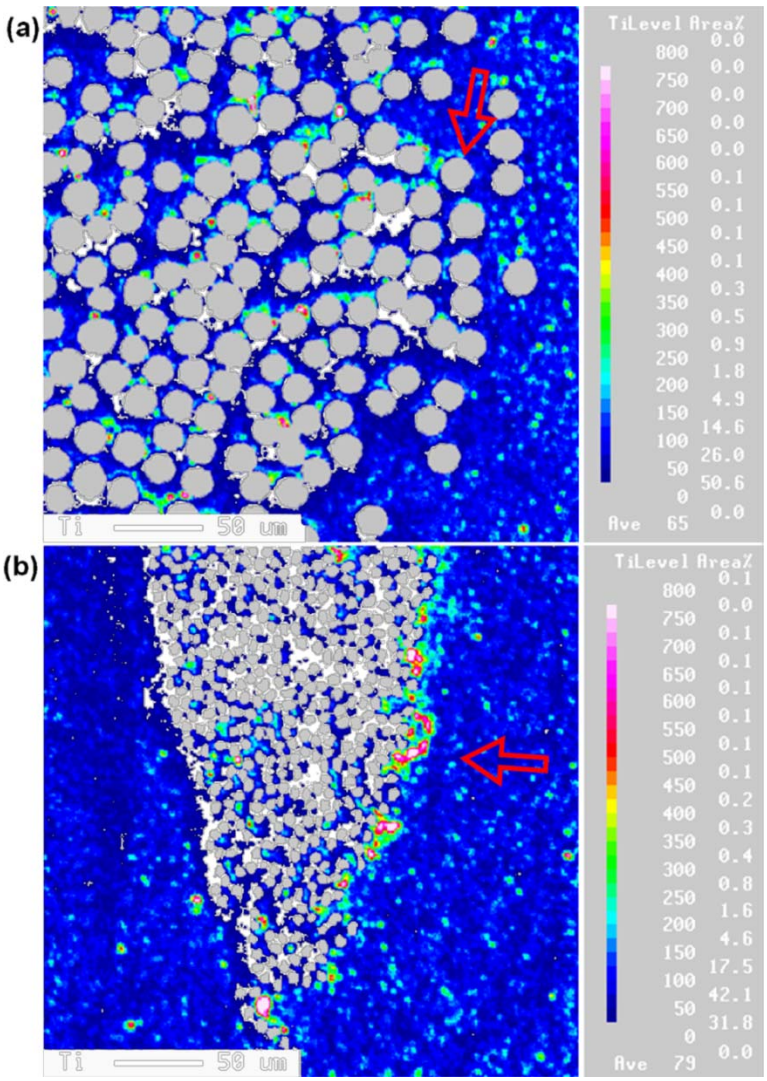

Figure 17 Distribution of TiO_2 particles in fiber-reinforced composite material, obtained by merging the elemental mapping results for the filler particles with the SEM image of the reinforcing fibers. (a) Exp. 1: 10 wt% spherical TiO_2 particles (d = 1 μm) and E-glass fibers. (b) Exp. 2: 10 wt% spherical TiO_2 particles (d = 1 μm) and carbon fibers.

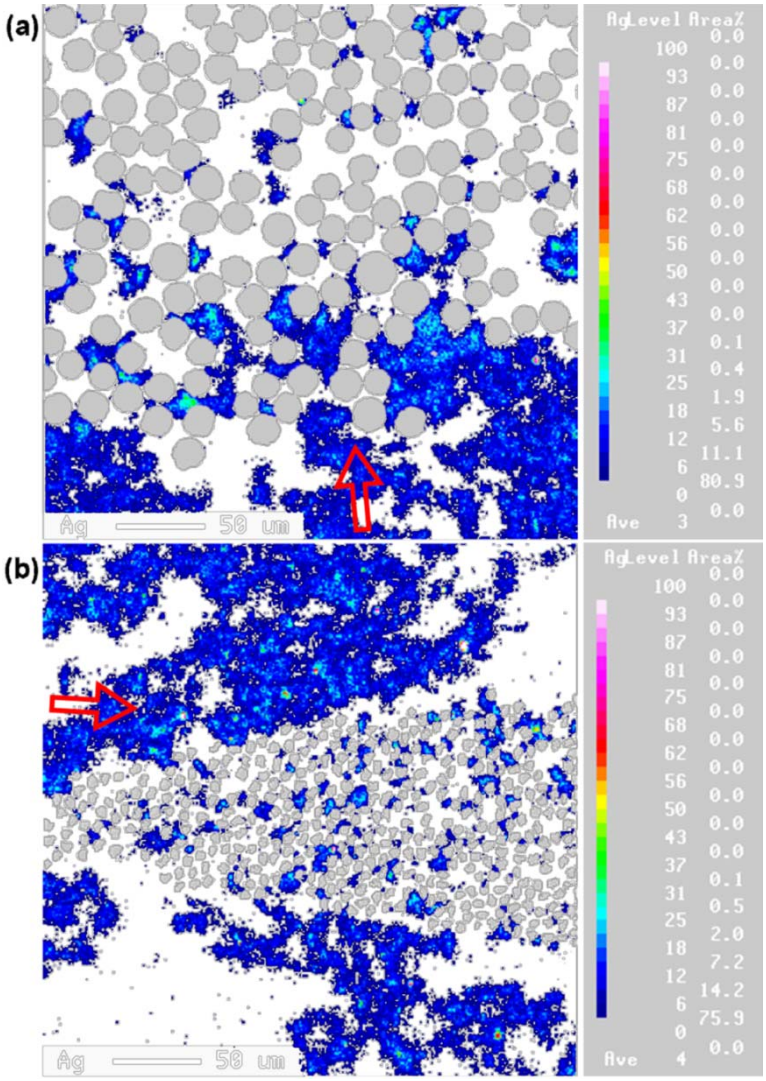

Figure 18 Distribution of CNT-silver particles in the fiber-reinforced composite material obtained by merging the elemental mapping results for the filler particles with the SEM image of the reinforcing fibers. (a) Exp. 3: 1 wt% CNT-silver particles and E-glass fibers. (b) Exp. 4: 1 wt% CNT-silver particles and carbon fibers.

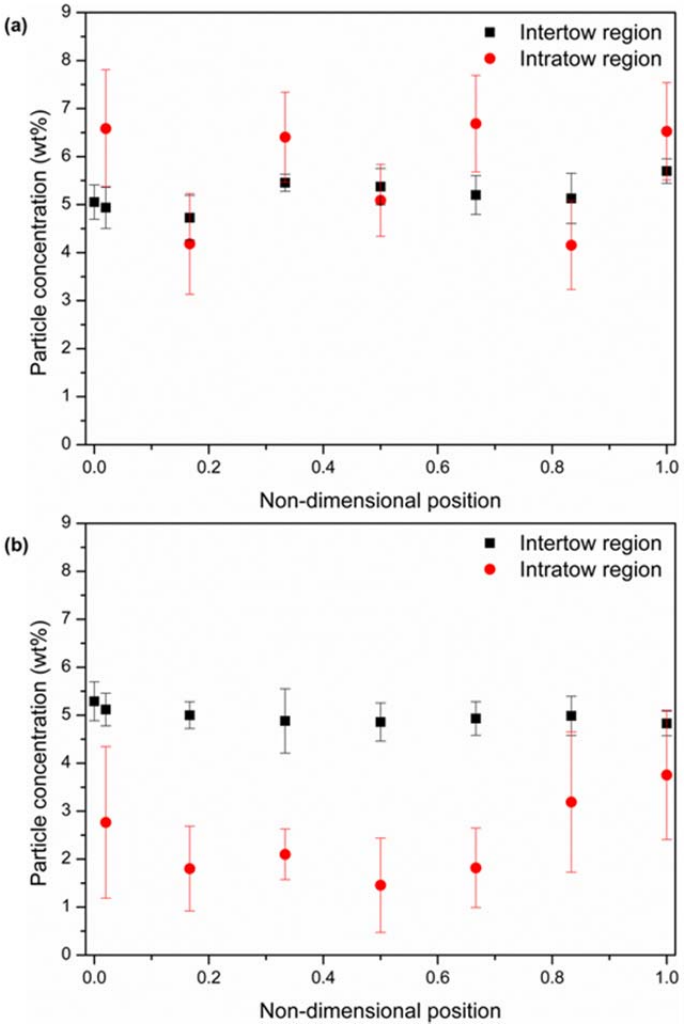

Figure 19 Concentration of TiO_2 particles in the fiber-reinforced composites in the intratow and intertow regions, in the injection direction of the suspension. (a) Exp. 1: 10 wt% spherical TiO_2 particles (d = 1 μm) and E-glass fibers. (b) Exp. 2: 10 wt% spherical TiO_2 particles (d = 1 μm) and carbon fibers.

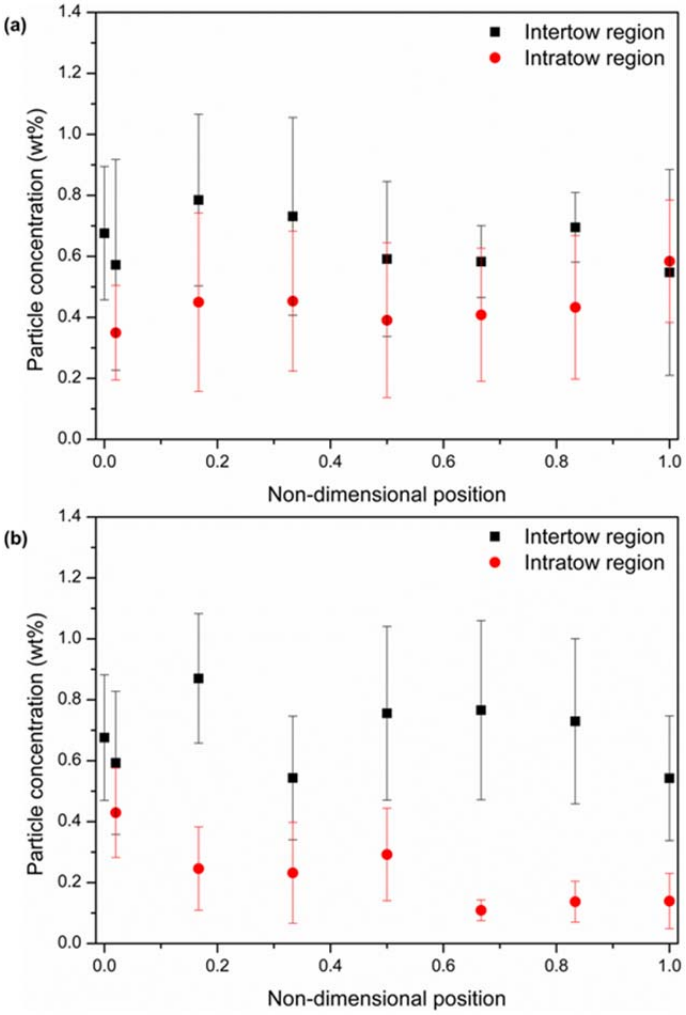

Figure 20 Concentrations of CNT-silver particles in the fiber-reinforced composite in the intratow and intertow regions, in the injection direction of the suspension. (a) Exp. 3: 1 wt% CNT-silver particles and E-glass fibers. (b) Exp. 4: 1 wt% CNT-silver particles and carbon fibers.

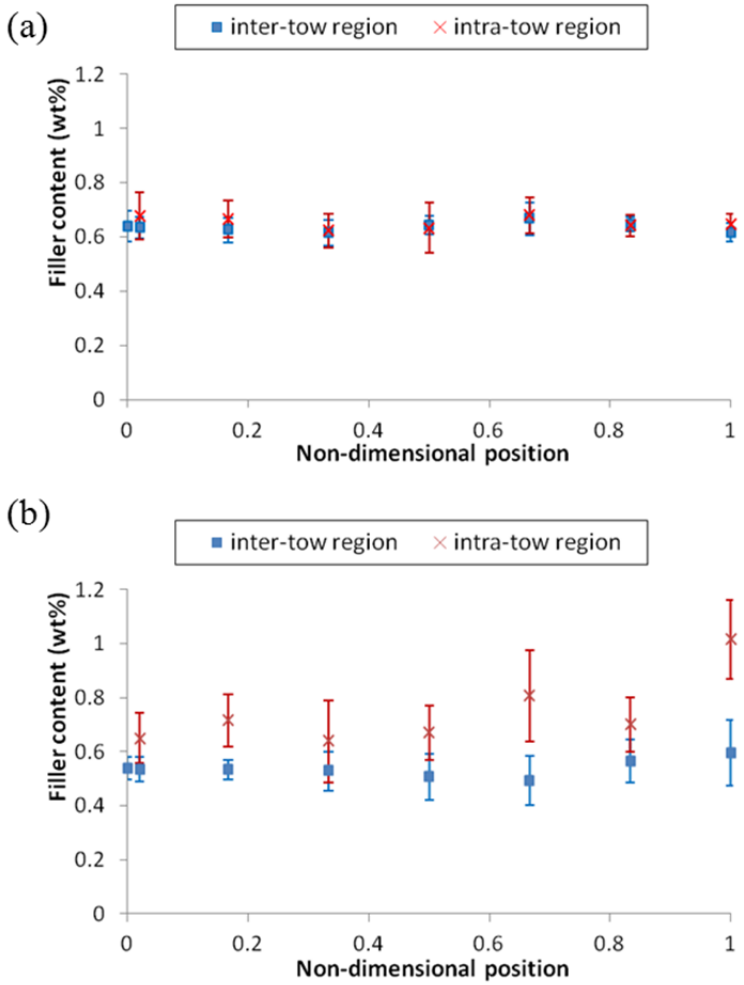

Figure 21 Concentration of TiO_2 particles in the glass fiber-reinforced composites in the intratow and intertow regions, in the injection direction of the suspension. (a) 1 wt% spherical TiO_2 particles (d = 32 nm). (b) 1 wt% spherical TiO_2 particles (d = 1 μm).

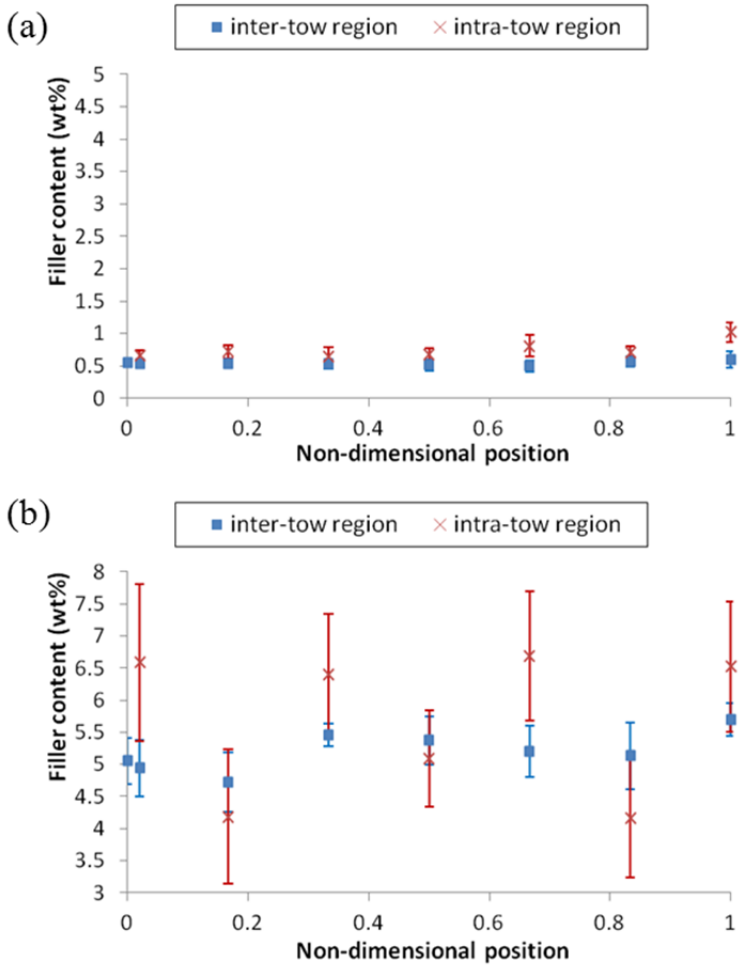

Figure 22 Concentration of TiO_2 particles with the diameter of 1 μm in the glass fiber-reinforced composites in the intratow and intertow regions, in the injection direction of the suspension. (a) 1 wt% spherical TiO_2 particles. (b) 10 wt% spherical TiO_2 particles.

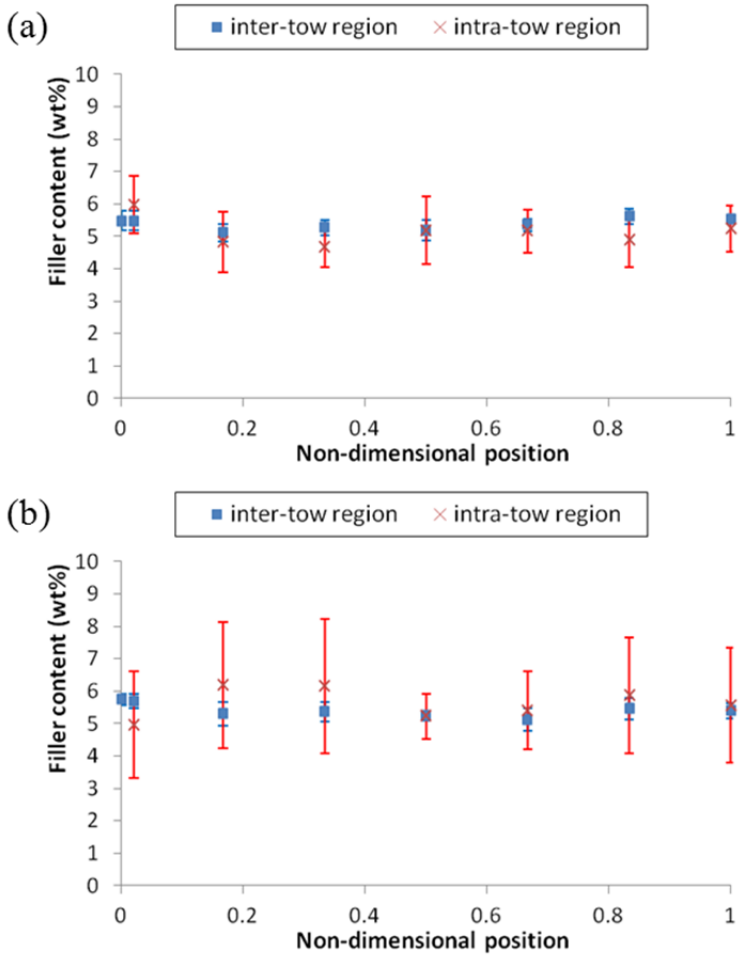

Figure 23 Concentration of TiO_2 particles with the diameter of 1 μm and initial concentration of 10 wt%, in the glass fiber-reinforced composites in the intratow and intertow regions, in the injection direction of the suspension. (a) fiber orientation is parallel to flow direction. (b) fiber orientation is normal to flow direction.

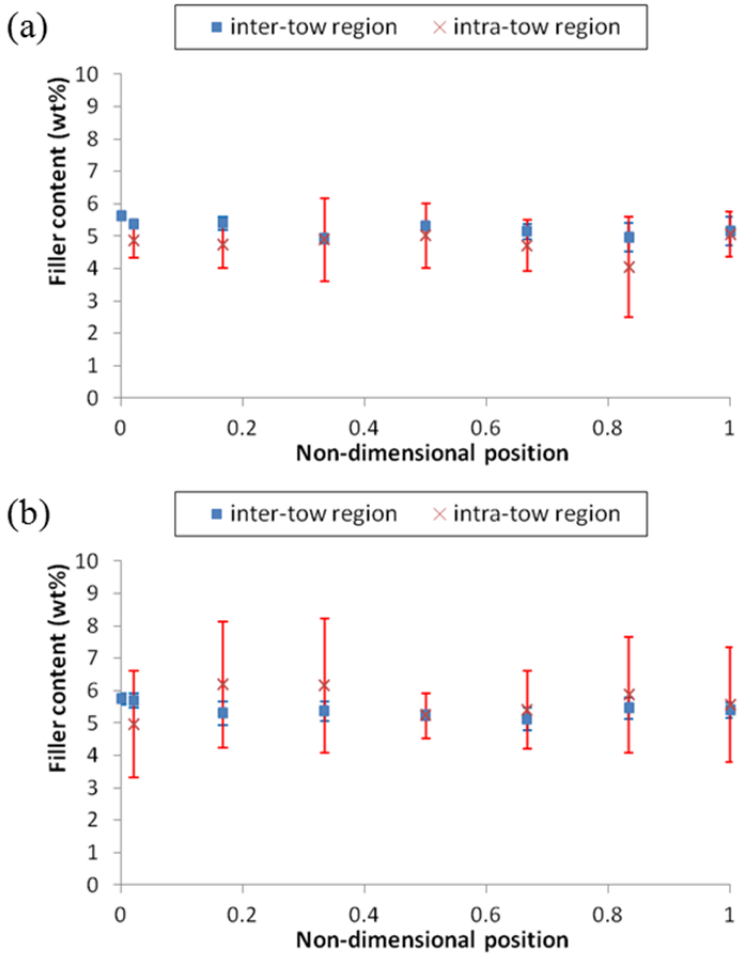

Figure 24 Concentration of TiO_2 particles with the diameter of 1 μm and initial concentration of 10 wt%, in the glass fiber-reinforced composites in the intratow and intertow regions, in the injection direction of the suspension. (a) the amount of injected suspension is 25 ml. (b) the amount of injected suspension is 100 ml.

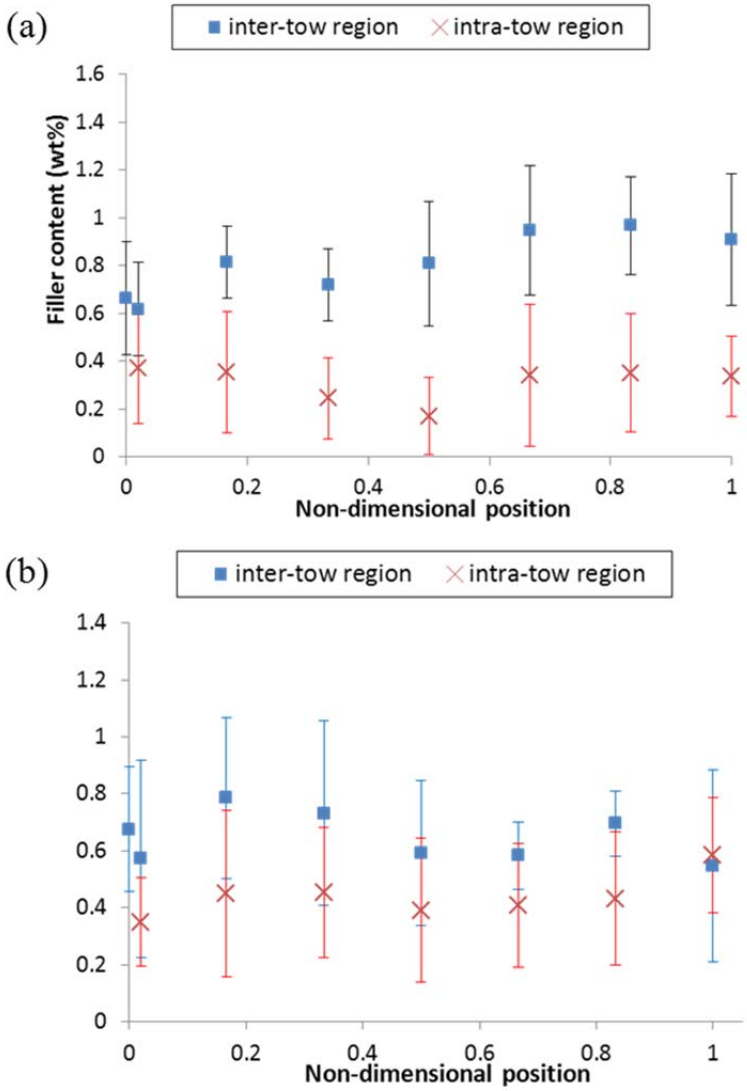

Figure 25 Concentrations of CNT-silver particles with the initial concentration of 1 wt% in the glass fiber-reinforced composite in the intratow and intertow regions, in the injection direction of the suspension. (a) dispersion time: 7 hours. (b) dispersion time: 20 hours.

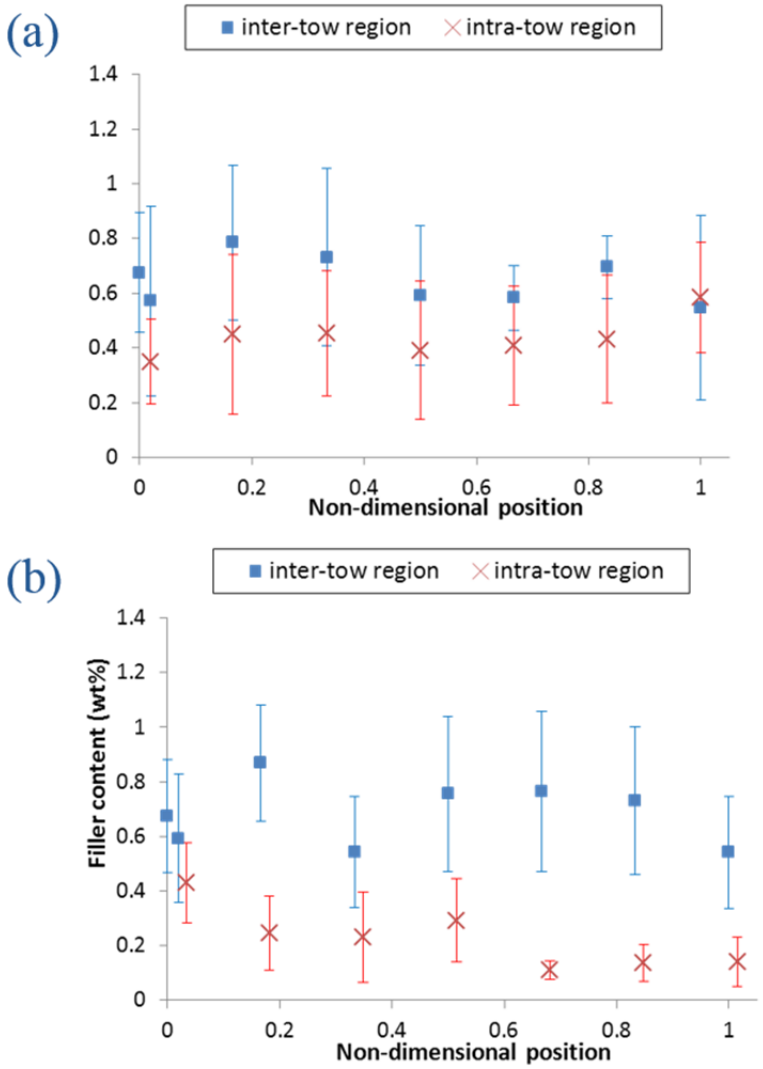

Figure 26 Concentrations of CNT-silver particles with the initial concentration of 1 wt% in the fiber-reinforced composite in the intratow and intertow regions, in the injection direction of the suspension. (a) Glass fibers (fiber volume fraction: 30%) (b) Carbon fiber (fiber volume fraction: 30%).

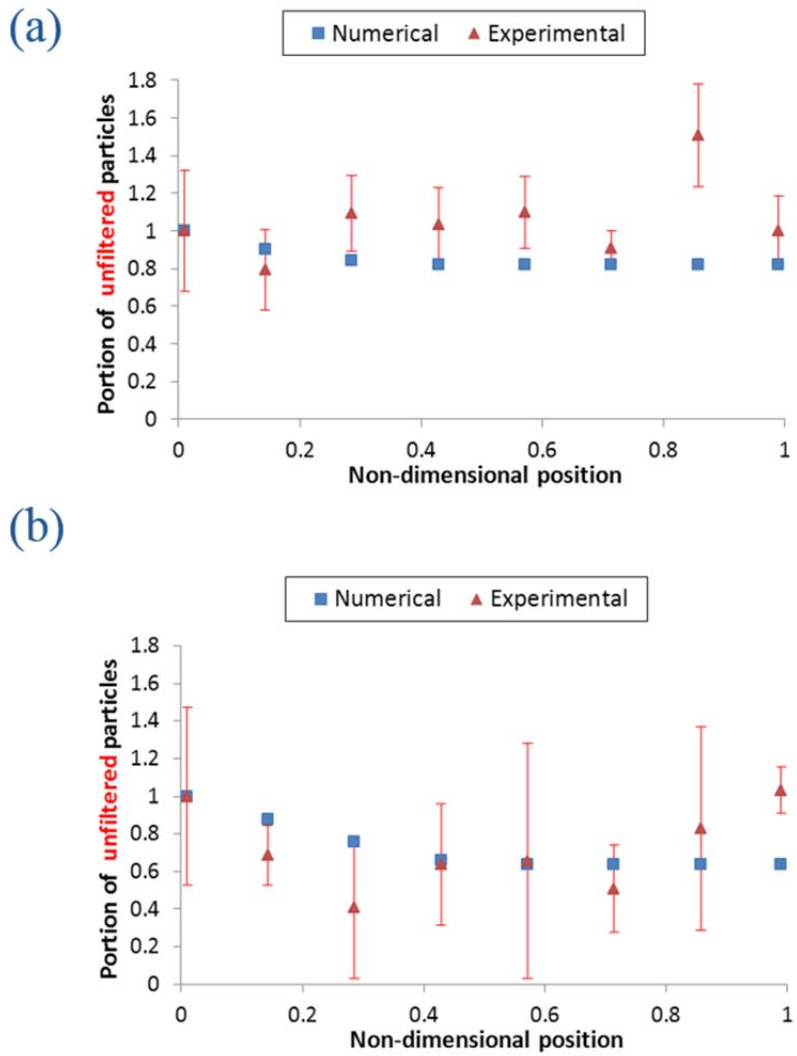

Figure 27 Experimental and numerical results of portion of unfiltered particles in the inter-tow region, in the injection direction of the suspension. (a) resin viscosity: 500 cP. (b) resin viscosity: 30 cP.

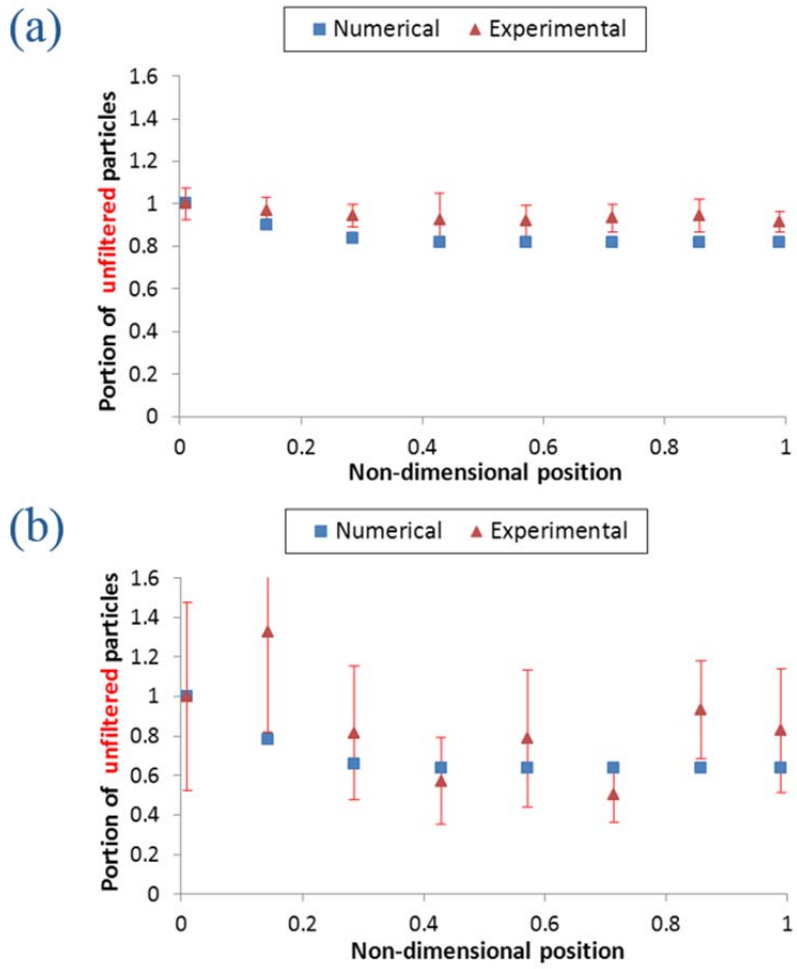

Figure 28 Experimental and numerical results of portion of unfiltered particles in the inter-tow region, in the injection direction of the suspension. (a) tow permeability: 3.00E-10 m^2. (b) tow permeability: 1.00E-9 m^2.

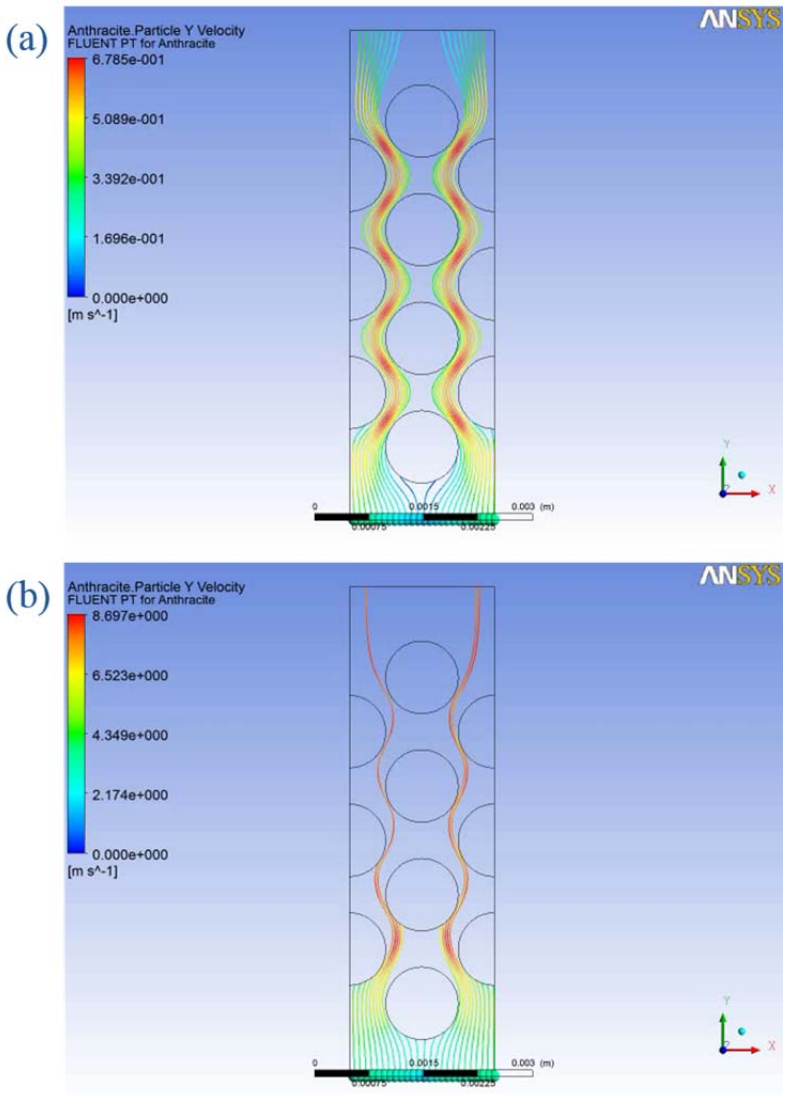

Figure 29 Numerical results of particle tracking solution. (a) resin viscosity: 500 cP. (b) resin viscosity: 30 cP.

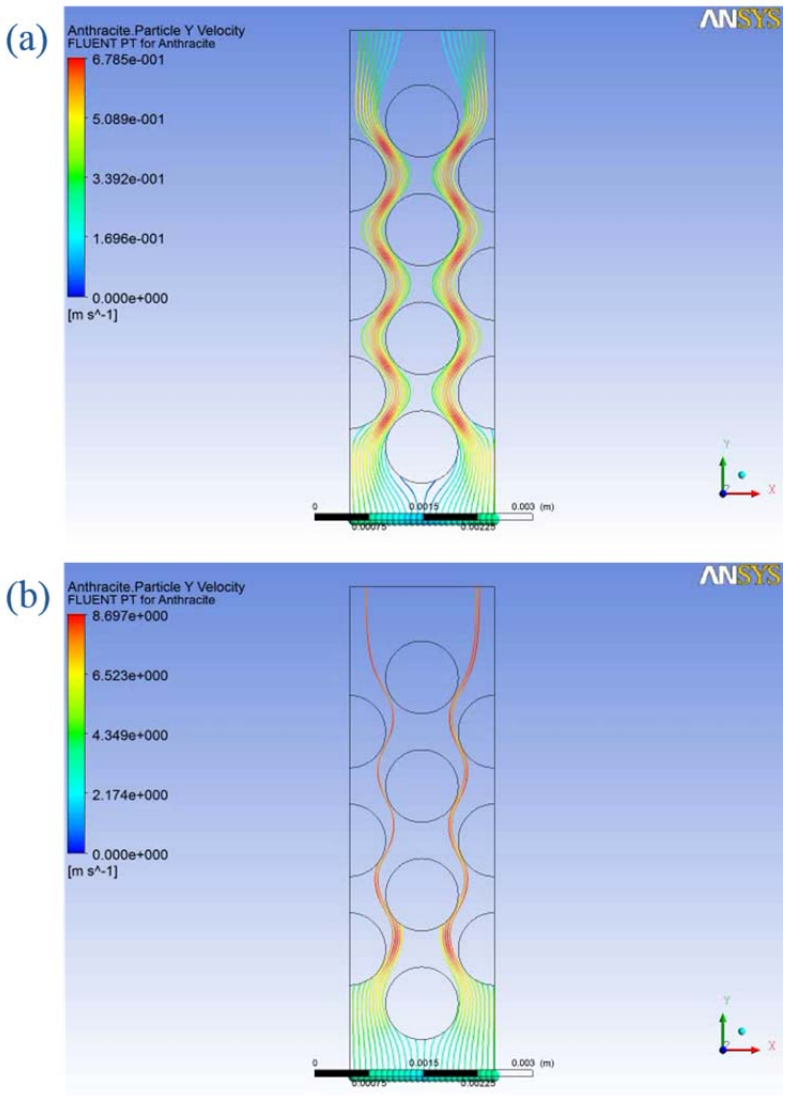

Figure 30 Numerical results of particle tracking solution. (a) tow permeability: 3.00E-10 m^2. (b) tow permeability: 1.00E-9 m^2.

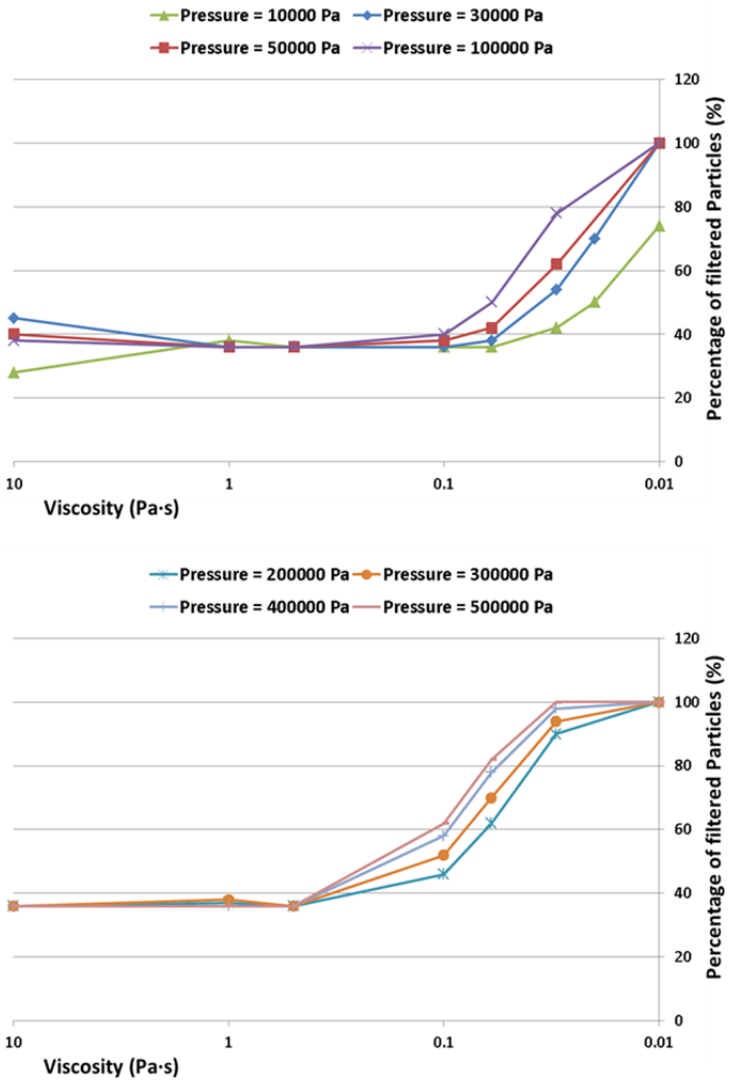

Figure 31 Numerical results of percentage of filtered particles at the boundary of the fiber tow for different resin viscosity

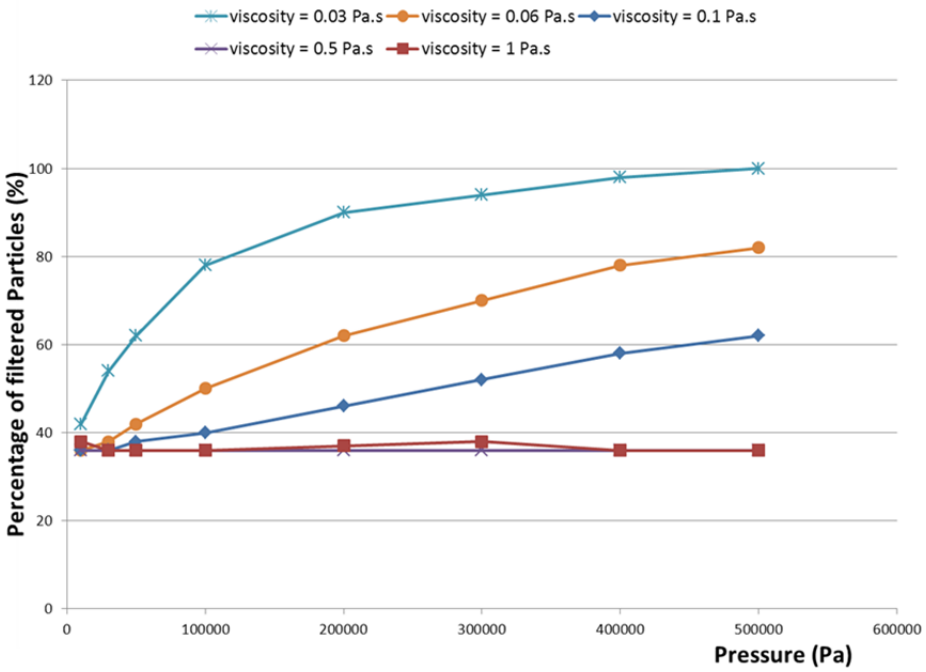

Figure 32 Numerical results of percentage of filtered particles at the boundary of the fiber tow for different injection pressure.

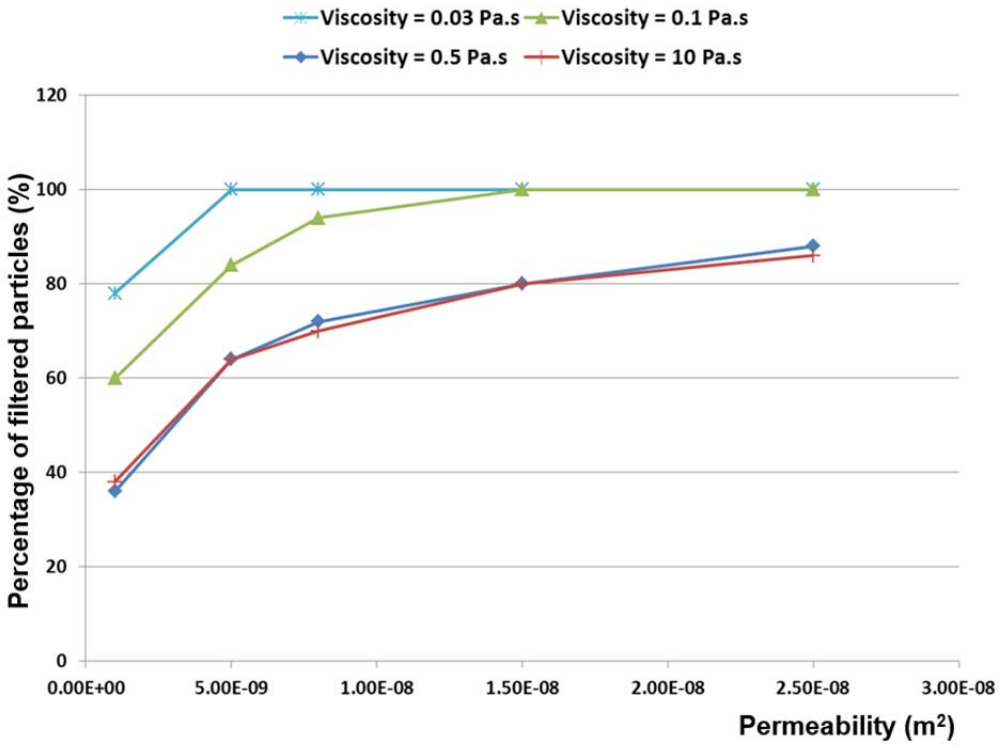

Figure 33 Numerical results of percentage of filtered particles at the boundary of the fiber tow for different tow permeability.

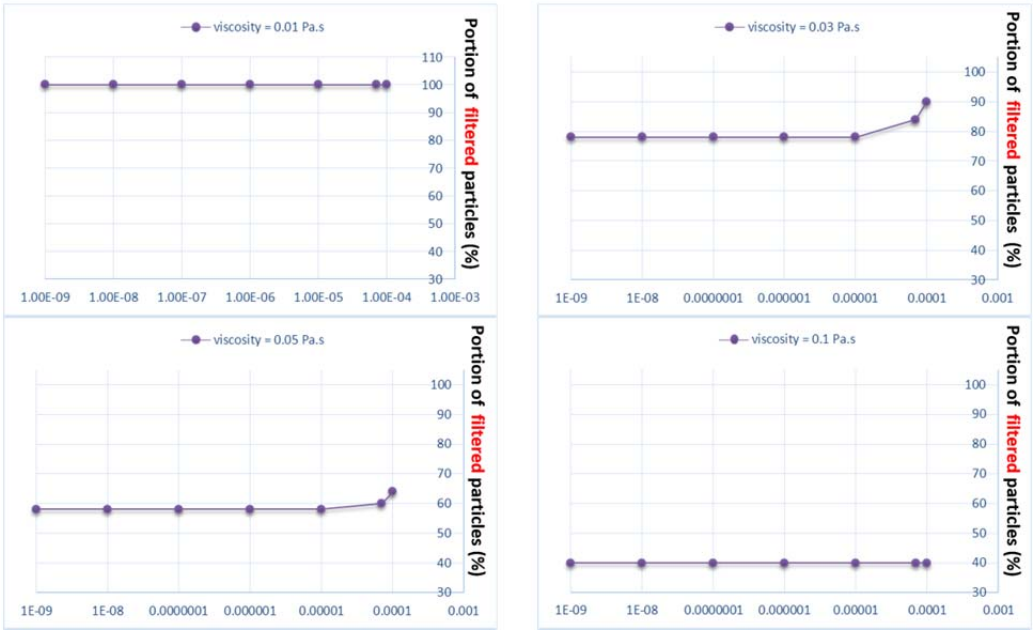

Figure 34 Numerical results of percentage of filtered particles at the boundary of the fiber tow for different particle diameter.

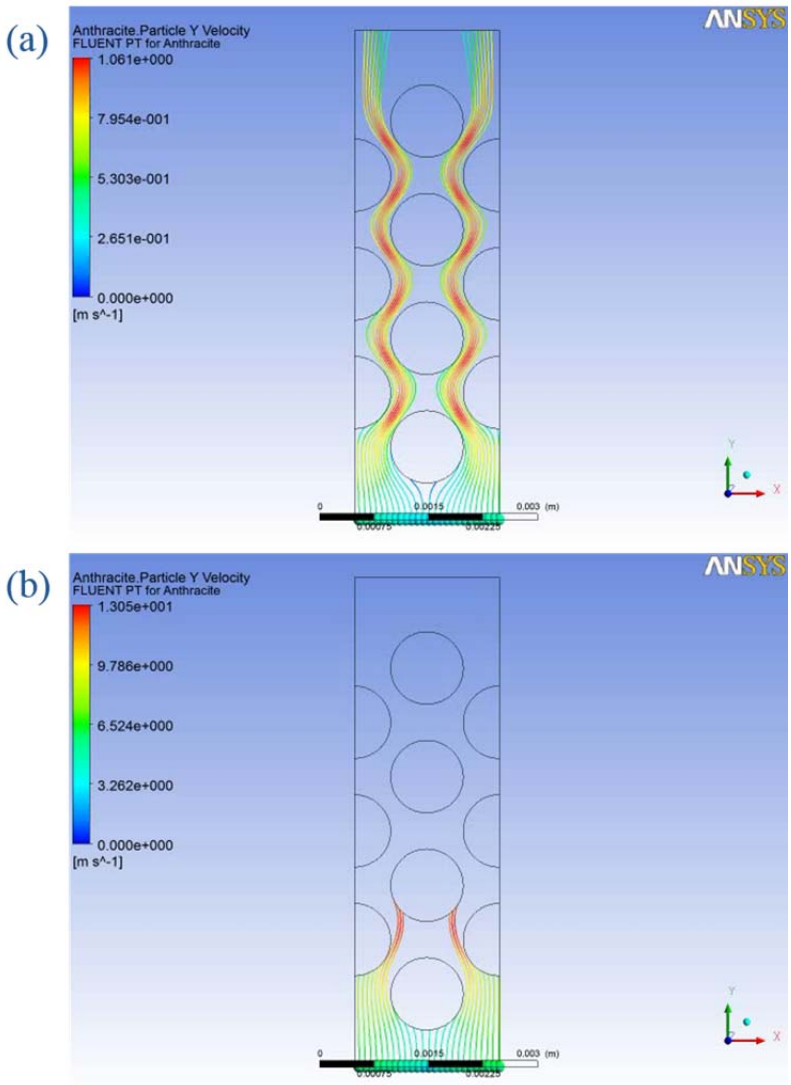

Figure 35 Numerical results of particle tracking solution in the case of resin viscosity of 30 cP. (a) Injection pressure: 0.1 atm. (b) Injection pressure: 4 atm.

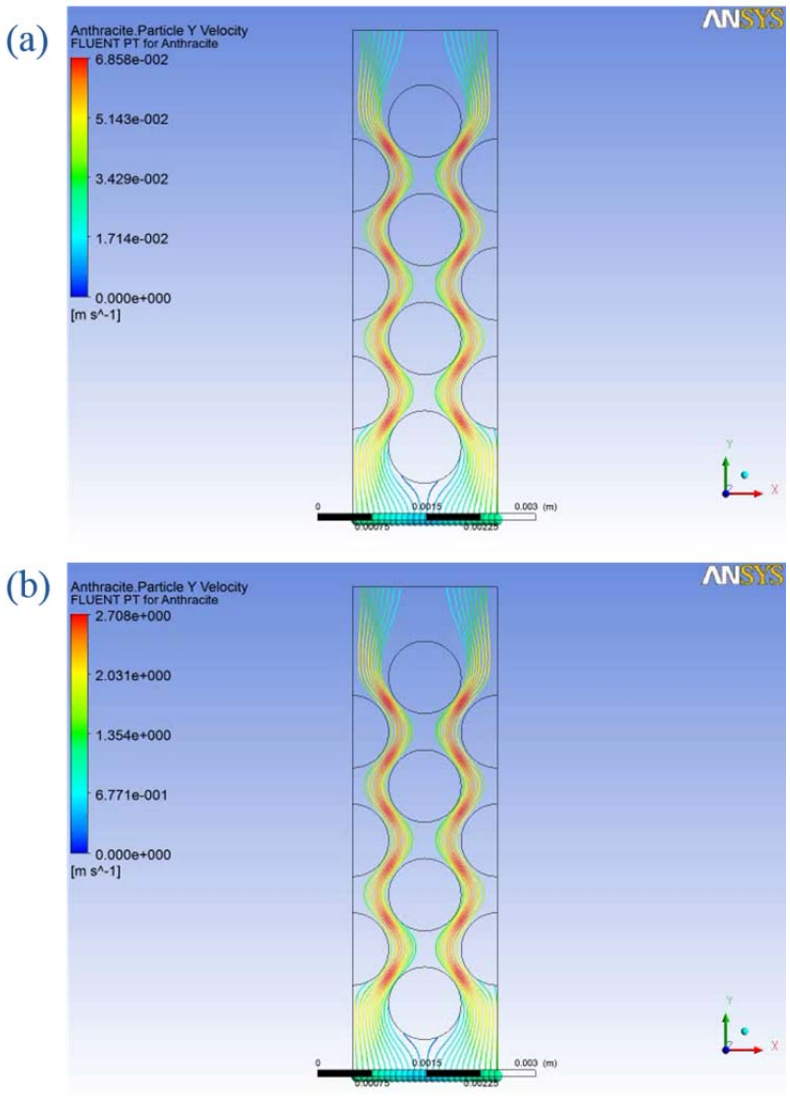

Figure 36 Numerical results of particle tracking solution in the case of resin viscosity of 500 cP. (a) Injection pressure: 0.1 atm. (b) Injection pressure: 4 atm.

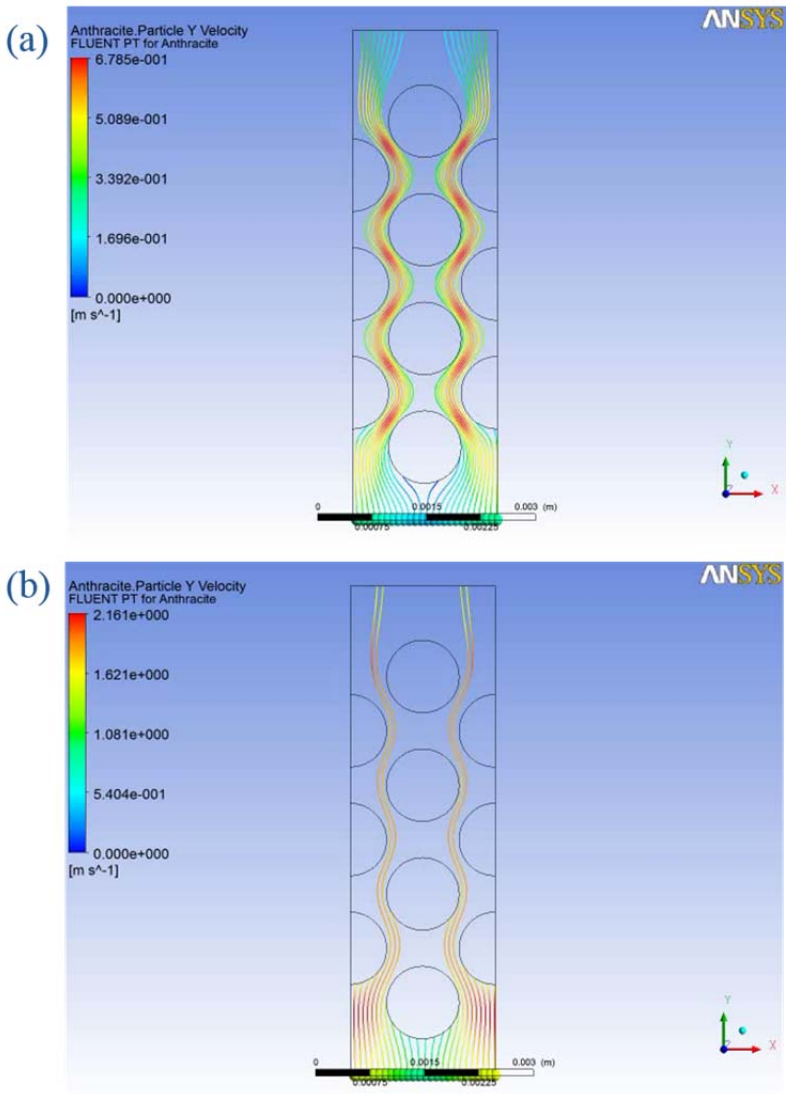

Figure 37 Numerical results of particle tracking solution. (a) tow permeability: 1.00E-09 m^2. (b) tow permeability: 1.50E-08 m^2.

x

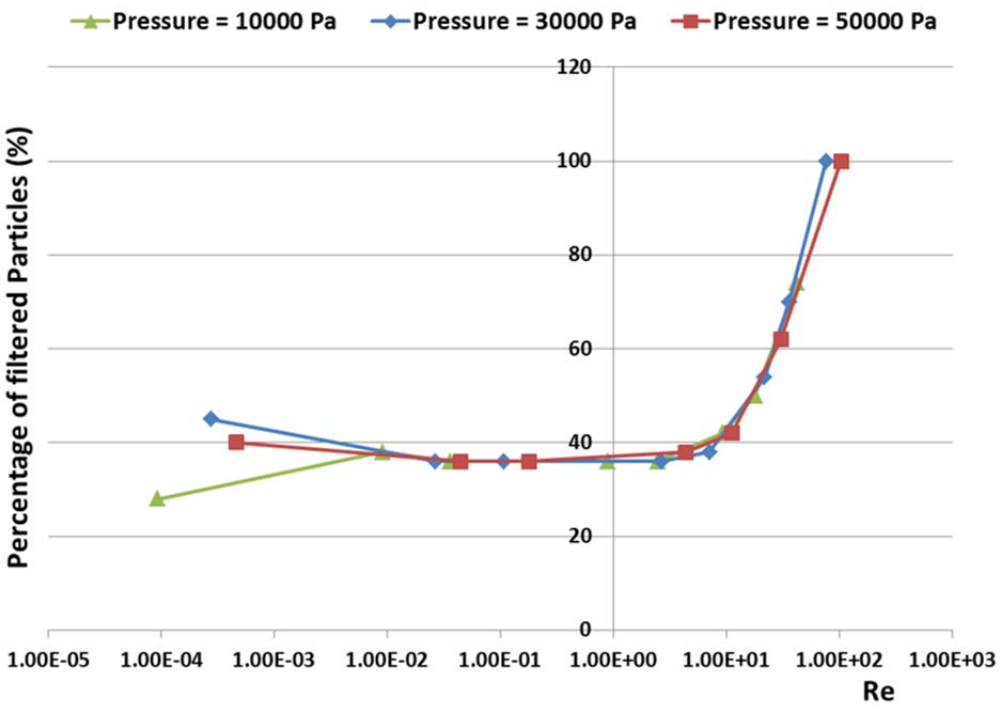

Figure 38 The percentage of filtered particles with respect to the Reynolds Number.

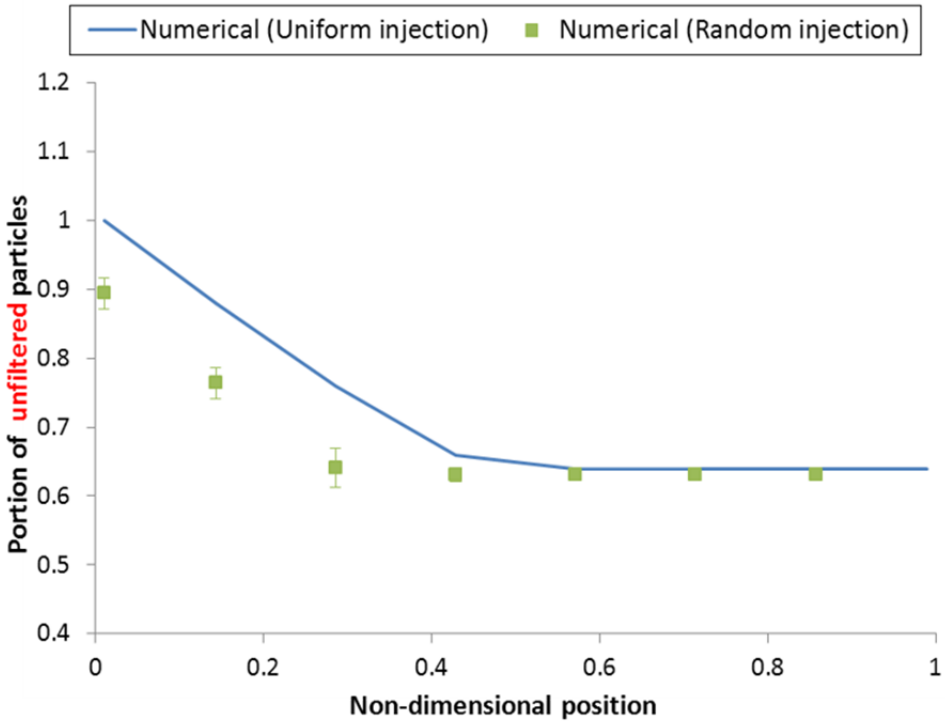

Figure 39 Numerical result of unfiltered particles distribution when the particles are injected with the random position at the injection line, and comparing with the experimental result.

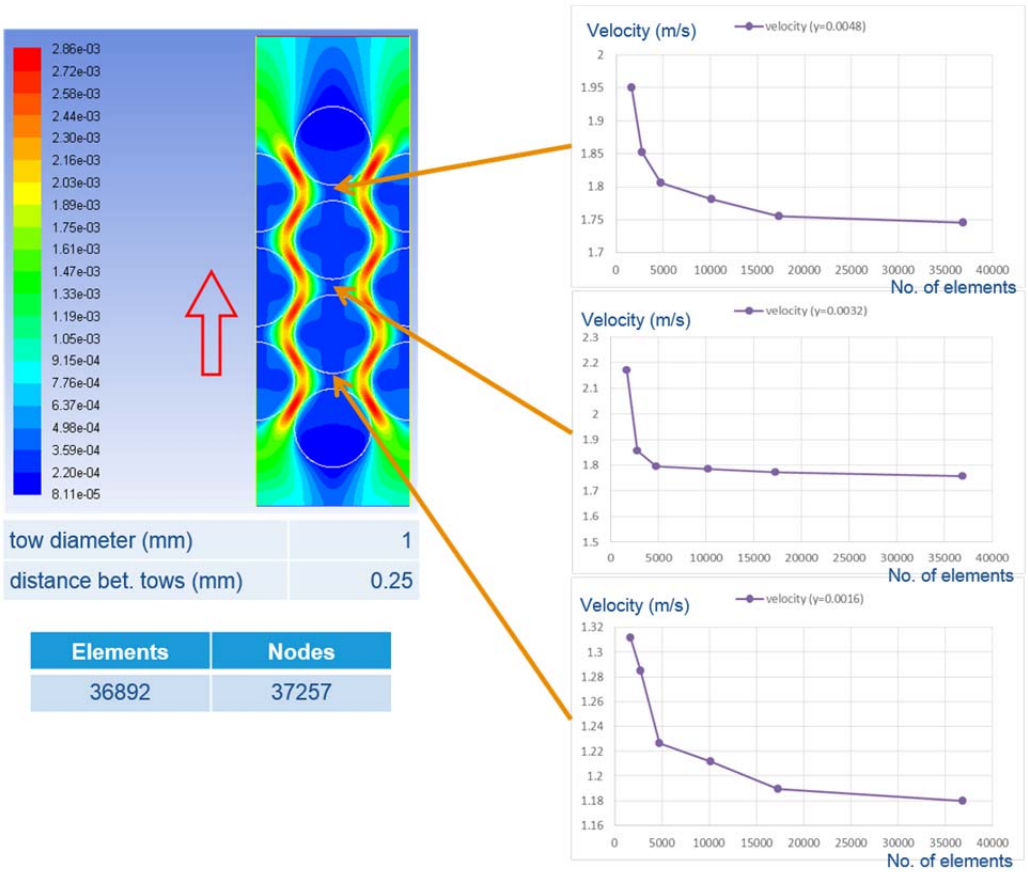

Figure 40 Mesh sensitivity – the velocity values obtained at the same point converge as the mesh size decrease.

Tables

Table 1 Selected features of the filler particles.

Filler Particle	Composition	Form	Diameter (Average)	Length (Average)
Titanium dioxide	TiO_2	Sphere	1 μm	-
CNT-silver	C	Tube	10–15 nm	10–20 μm
	Ag	Sphere	30 nm	-

Table 2 Material compositions of the composite parts used in this study

Exp. no.	Filler particle	Concentration (wt%)	Fibrous preform
Exp. 1	Spherical TiO_2 (d = 1 μm)	10	E-glass fiber
Exp. 2	Spherical TiO_2 (d = 1 μm)	10	Carbon fiber
Exp. 3	CNT-silver	1	E-glass fiber
Exp. 4	CNT-silver	1	Carbon fiber

Table 3 Parameter conditions of RTM manufacturing process (filler particle: TiO_2)

No.	Filler particles (Diameter)	Particle content	Ultrasonic process	Fiber volume fraction	Fiber orientation	Injection pressure	Amount of injected resin
Exp. 1	TiO_2 (32 nm)	1 wt%	10 hours	30 %	Parallel to flow	1 atm	100 ml
Exp. 2	TiO_2 (1 μm)	1 wt%	10 hours	30 %	Parallel to flow	1 atm	25 ml (Minimum)
Exp. 3	TiO_2 (1 μm)	1 wt%	10 hours	30 %	Parallel to flow	1 atm	100 ml
Exp. 4	TiO_2 (1 μm)	10 wt%	10 hours	30 %	Parallel to flow	1 atm	100 ml
Exp. 5	TiO_2 (1 μm)	10 wt%	10 hours	50 %	Parallel to flow	1 atm	100 ml
Exp. 6	TiO_2 (1 μm)	10 wt%	10 hours	50 %	Parallel to flow	2 atm	100 ml
Exp. 7	TiO_2 (1 μm)	10 wt%	10 hours	50 %	Normal to flow	2 atm	100 ml
Exp. 8	TiO_2 (1 μm)	10 wt%	10 hours	50 %	Normal to flow	2 atm	25 ml (Minimum)
Exp. 9	TiO_2 (1 μm)	10 wt%	10 hours	50 %	Normal to flow	2 atm	100 ml
Exp. 10	TiO_2 (1 μm)	10 wt%	10 hours	30 %	Woven carbon fiber	1 atm	100 ml

Table 4 Parameter conditions of RTM manufacturing process (filler particle: CNT-Ag)

No.	Filler particles (Diameter)	Particle content	Ultrasonic process	Fiber volume fraction	Fiber orientation	Injection pressure	Amount of injected resin
Exp. 1	CNT-Ag	1 wt%	7 hours	30 %	Parallel to flow	1 atm	100 ml
Exp. 2	CNT-Ag	1 wt%	20 hours	30 %	Parallel to flow	1 atm	100 ml
Exp. 3	CNT-Ag	1 wt%	20 hours	50 %	Parallel to flow	2 atm	100 ml
Exp. 4	CNT-Ag	1 wt%	20 hours	30 %	Woven carbon fiber	2 atm	100 ml

복합재료 액상 성형 공정에서 입자 필터링 현상에 대한 평가 및 모델링

서울대학교 대학원

기계항공공학부

염 상 혁

요약(국문초록)

기존의 복합재료 물성을 향상시키거나 새로운 기능을 가지는 복합재료를 개발하기 위해 다양한 형태의 미세 입자를 적용하려는 연구가 활발하게 진행되고 있다. 미세 입자가 첨가된 폴리머 수지를 이용하여 섬유 강화 복합재료를 생산하는 과정에서 입자의 필터링 현상이 발생하게 되며 이는 입자의 불균일한 분포와 재료의 결함을 가져오게 된다. 따라서 필터링 현상의 메커니즘을 이해하고 제어하는 기술을 개발하는 것이 중요한 연구 주제가 되고 있다. 본 연구에서는 전자현미분석기를 이용하여 경화된 복합재료 내의 첨가된 미세 입자의 함유량 및 분포를 마이크로 스케일에서 측정하는 방법을 제안하며, 구형 입자 및 은 나노 입자를 부착한 탄소나노튜브에 대하여 공정 변수에 따른 입자의 분포 양상을 측정하는 연구를 수행하였다. 강화 섬

유로 구성된 다공성 매질 내의 입자의 분포 및 농도 차이를 시각적으로 관찰할 수 있는 측정 방법과 정량 분석을 통한 재료 내에서의 공간적 분포 측정 방법을 제안하였다. 섬유 다발 내부와 외부의 이중 구조를 갖는 다공성 매질 내에서 두 영역 내의 입자 농도를 개별적으로 측정할 수 있었으며, 마이크로 스케일 뿐 아니라 나노 스케일의 입자에 대해서도 분석을 수행할 수 있었다. 제조 공정의 주요 변수들이 입자의 필터링 현상 및 분포에 미치는 영향에 대한 분석을 실험적 연구 및 수치 해석 연구를 병행하여 수행하였다.

주요어 : 입자 필터링, 나노복합재료, 전자현미분석기, 수지이송형성

학번 : 2008 – 30193

감사의 글

여호와는 나의 목자시니 내가 부족함이 없으리로다. 나의 평생에 선하심과 인자하심이 정녕 나를 따르리니 내가 여호와의 집에 영원히 거하리로다. (시편 23 1, 6절)

참으로 부족하고 허물 많은 저를 십자가에서 희생하신 놀라운 사랑으로 구원해 주시고, 선한 목자가 되어 주셔서 지금까지 저의 삶을, 특별히 박사과정 기간을 크신 은혜로 함께 하시고 양육해 주신 하나님께 감사를 드립니다. 박사과정을 마치며 남기는 이 작은 책보다도, 그 과정에서 경험했던 하나님의 사랑과 도우심의 기억들이 제게는 평생 믿음의 삶의 가장 귀한 자산으로 남을 것입니다.

짧지 않은 대학원 기간 동안 늘 따뜻한 관심과 많은 조언으로 저를 지도해 주신 이우일 교수님과 제게 아낌없는 도움과 기쁨을 주었던 연구실의 모든 동료와 후배들에게 감사의 인사를 올립니다. 기둥같이 항상 든든하게 연구실의 중심을 잡아준 민호형과 기주형, 가까이에서 누구보다 많은 대화로 마음을 나눴던 그리고 너무나 수고가 많았던 정우, 밝은 웃음과 성실함으로 보기만 해도 안심이 되는 든든한 성호와 형민이, 오랜 시간 함께 지내며 연구실의 흥망성쇠(?)를 함께 겪은 성하와 성남이, 늘 푸근한 골프채 전문가 재민이, 온갖 굳은 일을 도맡아 하면서도 마냥 즐거운 규희, 같은 믿음을 가져서 누구보다 편하고 좋았던 용철이, 남다른 센스로 즐거움을 줬던 범래, 그리고 미현, 다솜, 창기, 성학, 모든 신입 멤버들에게도 감사의 뜻을 전합니다. 지금은 연구실에 없지만, 가장 많은 훈계과 따뜻한 정을 베풀어 준 영석형, 큰 웃음과 따가운 책망을 함께 선사해 준 동언형, 그리고 아는 것 없이 헤메고 있을 때 정성으로 이끌어 주었던 승모형, 성웅형, 시환형, 재원형, 그리고 저에게 많은 도움을 주신 김한상 교수님과 그 외 모든 선배들께도 고마운 마음을 전하고 싶습니다.

대학원 기간 동안 저의 믿음의 삶에 소중한 도움을 주신 많은 분들께 감사의 인사를 올립니다. 일평생 한결같은 믿음과 섬김으로 아름다운 열매와 귀한 본을 보여주시고 사랑과 격려를 아낌없이 베풀어 주신 하선생님 내외분께 진심으로 감사를 드

립니다. 흠 많고 연약한 저의 모습을 사랑으로 용납하시고 이제까지 은혜와 진리로 양육해 주시고 세워주신 김상완 형제님과 철원형, 호석형께 감사를 드립니다. 날로 어지러워지는 세상에서 제게 흔들림 없는 분명한 믿음의 삶의 방향을 제시해 주시는 이건도, 이준호, 임세범, 윤준호 형제님들께도 감사의 인사를 드립니다. 함께 팀웍하며 귀한 본과 조언과 즐거움으로 섬겨주신 임유신, 문준희, 원남일 형제님들과 혁준형께도 진심으로 감사를 드립니다. 따뜻하게 격려해 주시고 잘 가르쳐 주신 문호석 형제님, 오랜 시간 함께 살며 따뜻한 정을 베풀어 준 용관형, 유쾌한 웃음과 예리한 조언으로 필요를 채워준 한준형, 말씀과 사랑으로 가까이서 많은 도움을 주었던 한이형, 결코 예외를 두지 않는 섬김으로 산 교훈을 준 동희형, 같은 학번과 같은 학과에서 함께 믿음을 나누며 도전과 기쁨을 주었던 성익에게도 감사의 뜻을 표합니다. 깨끗한 믿음과 순수한 열정으로 기쁨이 되어 준 사랑하는 은상이, 열정으로 배우고 섬기는 영원한 학부생 경환이, 묵묵하면서도 유쾌하고 확신 넘치는 정훈이, 그리스도의 군사로 즐거이 헌신하는 세진이와 지용이, 한국인보다 더 한국인같은 이 시대의 아브라함 야마다아키히코, 쉽지 않은 공부를 감당하며 먼 곳에서 오가며 배우느라 수고한 현진이, 팀에 신선한 활력과 기쁨이 되어 준 그리고 나에게 운동하는 즐거움을 새롭게 깨우쳐 준 영기와 선우, 온유한 군인 동제와 함께 주님 안의 기쁨을 나눠 온 현종, 두현에게도 감사의 인사를 전합니다. 또한 함께 생활하며 귀한 말씀과 조언으로 가르쳐주고 따뜻한 관심과 사랑으로 섬겨준 현표형, 지훈형, 준영형에게도 참으로 감사를 드립니다.

마지막으로 제가 이 자리에 있기까지 사랑과 헌신으로 낳아주고 길러주시고 늘 부족한 아들에게 더 많이 베풀어주시는 사랑하는 아버지와 어머니, 누구보다 많은 기도로 저를 지원해 주시는 사랑하는 할머니, 나와서 살고 있는 형 대신 집안의 기둥 역할을 하며 착하게 형을 잘 따라준 동생 주혁이에게도 진심으로 감사의 인사를 드립니다.

2014년 2월 3일